Climate Dynamics (1994) 10:107–134

Climate Dynamics

The global heat balance: heat transports in the atmosphere and ocean

Kevin E. Trenberth, Amy Solomon*

National Center for Atmospheric Research, P.O. Box 3000, Boulder, CO 80307, USA

Received: 13 August 1993/Accepted: 22 December 1993

Abstract. The heat budget has been computed locally over the entire globe for each month of 1988 using compatible top-of-the-atmosphere radiation from the Earth Radiation Budget Experiment combined with European Centre for Medium Range Weather Forecasts atmospheric data. The effective heat sources and sinks (diabatic heating) and effective moisture sources and sinks for the atmosphere are computed and combined to produce overall estimates of the atmospheric energy divergence and the net flux through the Earth's surface. On an annual mean basis, this is directly related to the divergence of the ocean heat transport, and new computations of the ocean heat transport are made for the ocean basins. Results are presented for January and July, and the annual mean for 1988, along with a comprehensive discussion of errors. While the current results are believed to be the best available at present, there are substantial shortcomings remaining in the estimates of the atmospheric heat and moisture budgets. The issues, which are also present in all previous studies, arise from the diurnal cycle, problems with atmospheric divergence, vertical resolution, spurious mass imbalances, initialized versus uninitialized atmospheric analyses, and postprocessing to produce the atmospheric archive on pressure surfaces. Over land, additional problems arise from the complex surface topography, so that computed surface fluxes are more reliable over the oceans. The use of zonal means to compute ocean transports is shown to produce misleading results because a considerable part of the implied ocean transports is through the land. The need to compute the heat budget locally is demonstrated and results indicate lower ocean transports than in previous residual calculations which are therefore more compatible with direct ocean estimates. A Poisson equation is solved with appropriate boundary conditions of zero normal heat flux through the continental boundaries to obtain the ocean heat transport. Because of the poor observational data base, adjustments to the surface fluxes are necessary over the southern oceans. Error bars are estimated based on the large-scale spurious residuals over land of 30 W m^{-2} over 1000 km scales (10^{12} m^2). In the Atlantic Ocean, a northward transport emerges at all latitudes with peak values of 1.1 ± 0.2 PW (1 standard error) at 20 to 30°N. Comparable values are achieved in the Pacific at 20°N, so that the total is 2.1 ± 0.3 PW. The peak southward transport is at 15 to 20°S of 1.9 ± 0.3 PW made up of strong components from both the Pacific and Indian Oceans and with a heat flux from the Pacific into the Indian Ocean in the Indonesian throughflow. The pattern of poleward heat fluxes is suggestive of a strong role for Ekman transports in the tropical regions.

Introduction

It is widely recognized that the differential heating between the low and high latitudes is the primary driving force for the the atmospheric circulation on all time scales. Satellite measurements of the Earth radiation budget have clearly revealed the surplus of incoming absorbed solar over outgoing longwave radiation in low latitudes, while the reverse is true at high latitudes on an annual mean basis (e.g., Fig. 1). Thus, radiative processes are continually acting to cool the high latitudes and warm the low latitudes, and it is only the poleward heat transport by the atmosphere and the oceans that serves to offset this. Beyond these general statements, our detailed knowledge of the exact distribution of heating, how that breaks down into radiative, sensible and latent heating components, and the processes involved in redistributing heat is far from complete.

The critical poleward transports of heat are partitioned between the atmosphere and the ocean. Conventional wisdom has maintained that our knowledge

* *Present address:* Center for Meteorology and Physical Oceanography, Massachusetts Institute of Technology, Cambridge, MA02139

Correspondence to: K. E. Trenberth

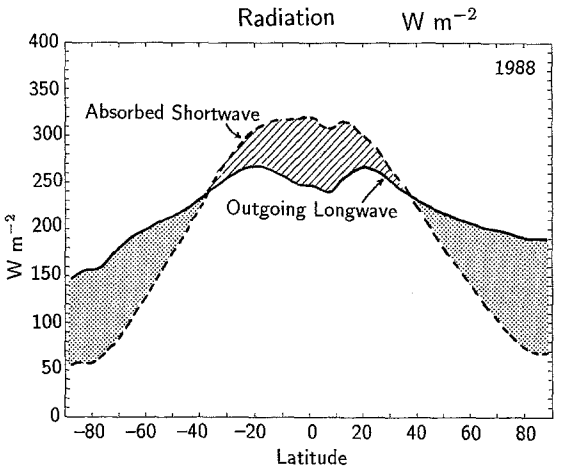

Fig. 1. Zonal mean top-of-the-atmosphere radiation from ERBE for 1988 as a function of latitude in W m^{-2}. Shown are the absorbed shortwave and outgoing longwave radiation, with their difference highlighted to show the excess in the tropics and deficit at high latitudes

of the atmospheric transports is sufficient that it can be combined with satellite measurements of the radiative components to deduce the ocean heat transports as a residual. Yet results do not correspond well with the few independent estimates of the ocean heat transport. In this study, therefore, we critically reexamine the heat balance locally over the entire globe for the year 1988 and we attempt to assess what confidence can be placed in the heating and heat transport in the atmosphere, and thus assess how well we can establish the net heat flux through the bottom of the atmosphere that implicitly determines the oceanic heat transport.

Communication between the atmosphere and ocean is through the fluxes of heat, fresh water and momentum and knowledge of the atmospheric-ocean exchanges is critical for atmosphere-ocean modeling. Atmospheric GCMs (general circulation models) are developed using specified lower boundary conditions [sea surface temperatures (SSTs), etc.] which provides a strong constraint on the modeled atmosphere. Ocean GCMs are developed with either a specified surface atmosphere, specified fluxes and/or relaxation to observed surface temperature and salinity. These provide a strong constraint on the ocean component. Thus, the component models have their own systematic errors and consequently coupled atmosphere-ocean models drift to a new model climate if left alone. Even small errors in one component model can be amplified by feedbacks. Widespread use has been made of unphysical "flux correction" to offset such drift and keep the modeled surface conditions similar to observed. The fluxes corrected include heat, fresh water, and momentum (or a subset of these). However, the observational evidence to evaluate the models and the corrections is insufficient at present. It is, therefore, important to improve knowledge of "observed" surface ocean fluxes to increase our understanding of the coupled system and improve coupled models.

Atmosphere-ocean fluxes may be inferred using bulk methods and observed surface variables (for instance Hastenrath 1980, 1982; Hsiung 1985; Isemer and Hasse 1987; Oberhuber 1988). From these methods it is possible to obtain reasonable estimates of patterns of sensible and latent heat exchange, but substantial (several tens of W m^{-2}) systematic errors arising from the parameterizations, sampling and uncertainties in the exchange coefficients are probable (e.g., Weare and Strub 1981; Weare 1989). Estimates of surface radiation depend heavily on ship cloud observations which are poor from the surface, and the various empirical formula can err by up to 32% (Dobson and Smith 1988), so this component is quite uncertain. Estimates of surface wind stress also appear to be reasonable, but again systematic errors exist (e.g., Trenberth et al. 1990). All these fluxes strongly depend on adequate sampling, and insufficient sampling exists over most of the southern ocean in particular (Trenberth et al. 1990).

As noted above, an alternative method, to be exploited here, relies on indirect estimates of the surface heat exchange as a residual of the top-of-the-atmosphere satellite observed net radiation and the divergence of the energy transports from global atmospheric analyses from the atmospheric heat and moisture budgets. Given the surface flux, ocean heat transports may also be estimated. Errors exist in both components but the Earth Radiation Budget Experiment (ERBE) has allowed the radiation errors to be much better quantified. In principle the errors in this method as a whole can be quantified by carrying out analysis over land where below ground energy transports must be small. In practice, however, the added complications of complex orography and treatment of the atmospheric lower boundary mean that conclusions drawn from land residuals do not necessarily apply over the oceans (see third section).

The focus, therefore, is on the annual mean atmospheric heat budget to provide updates to the earlier studies of Vonder Haar and Oort (1973), Oort and Vonder Haar (1976) for the Northern Hemisphere (NH) and Trenberth (1979) for the Southern Hemisphere (SH). These studies and more recent estimates by Carissimo et al. (1985) and Savijärvi (1988) made use of radiosonde data, but the uncertainties in the atmospheric heat transports are substantial. This is obvious at 70°S in the Carissimo et al. (1985) and Savijärvi (1988) results, for instance, where there is no ocean but their residuals imply a large poleward heat transport by the ocean. Problems are especially evident arising from estimates of atmospheric divergence in low latitudes in the rawinsonde-based analyses, but this aspect seems to be improving steadily in global analyses.

Thus, an alternative approach is to use state-of-the-art global analyses to assess the atmospheric heat transports (Boer 1986; Masuda 1988), as has been recently done by Michaud and Derome (1991). The quality of atmospheric analyses produced from four-dimensional data assimilation systems has continued to im-

prove in spite of observational losses (e.g., Trenberth 1992; Trenberth and Olson 1988). Consequently it is generally considered desirable to use the most recent analyses available to compute the atmospheric heat transports. Top-of-the-atmosphere heat budget information derived from satellite is necessary to complete the atmospheric heat budget and it is important to have data for the same months for the results to be valid locally. Therefore use is made of ERBE results for which the most recent year with sufficient quality is 1988 (see fourth section).

Stone and Risbey (1990) have examined atmospheric GCM heat transports and compared with "observed" as given by Carissimo et al. (1985), and concluded that most atmospheric GCM heat transports are deficient. However, an alternative conclusion is that the "observations" are deficient. We believe this to be the case (see Boer 1986), although it does not exclude the possibility that GCM transports may also be flawed. In this study we provide an update of recent heat transport estimates and an assessment of the sources of errors.

The approach uses the global analyses for 1988 from the European Centre for Medium Range Weather Forecasts (ECMWF) but with assessments of the impacts of changes in the analysis system and the characteristics of the analyses on the implied transports. There are major uncertainties at low latitudes owing to the ever-changing character of the global analyses (Trenberth 1992), which is manifested, in particular, in the changing strength of the analyzed mean meridional circulation. Substantial changes have occurred since 1988. Other issues include differences among analyzed data sets, such as those from different centers, two versus four times per day analyses which determine how well the diurnal cycle is resolved, whether the analyses are initialized or uninitialized, and issues of vertical resolution, and these are all discussed later. It appears that no past studies have carried out a proper treatment of the lower boundary as described in Trenberth (1991). The goal is to gain a better appreciation for where the uncertainties lie and which aspects we can trust.

Data sets

The radiation data and its processing is discussed in the fourth section. Use is made of the ERBE dataset of monthly means which has been processed onto a T42 Gaussian grid by Hurrell and Campbell (1992).

Global analyses of various quantities are needed to carry out the diagnostic studies. The most convenient global data sets for this purpose are the global analyses produced operationally for weather forecasting purposes (Fortelius and Holopainen 1990). These are produced using a four-dimensional (4-D) data assimilation system in which multivariate observed data are combined with the "first guess" using a statistically optimum scheme. The first guess is the best estimate of the current state of the atmosphere from previous analyses produced using a numerical weather prediction (NWP) model.

The global atmospheric analyses produced as a result of four-dimensional data assimilation operationally consist of global fields of northward and eastward wind components (u, v), geopotential height (z), temperature (T), and relative humidity (RH) or, equivalently, specific humidity (q) each of which are a function of pressure (p). ω (vertical p-velocity) fields are produced diagnostically from the equation of continuity. In recent times, these quantities have been analyzed on the levels of the numerical weather prediction model used in the 4-D data assimilation to provide the first guess for the analyses. Generally, these are σ levels where $\sigma=p/p_s$, and p_s is the surface pressure defined on the model surface topography. Alternatively, a hybrid between σ and pressure coordinates is used which typically reverts to constant pressure above about 100 mb. Analyzed fields on standard constant pressure levels are produced by interpolation. Actually, the changes in the analysis from one synoptic observation time to the next are interpolated to update the standard pressure level fields (after November 1984 at ECMWF), though the details as to how this has been done have changed with time. Once the fields have been analyzed, they are typically initialized to bring the mass and temperature fields into a dynamical balance with the velocity fields consistent with the predominant low frequency motions in the atmosphere.

It must be emphasized that the operational analyses are performed under time constraints for weather forecasting purposes and not for climate purposes. Changes in the NWP model, data handling techniques, initialization, and so on, which are implemented to improve the weather forecasts, may disrupt the continuity of the analyses (Trenberth and Olson 1988; Trenberth 1992). Two datasets have been used, one with twice-daily initialized analyses at seven levels in the vertical (1000, 850, 700, 500, 300, 200 and 100 mb), the other with four-times daily uninitialized analyses at 14 levels (1000, 850, 700, 500, 400, 300, 250, 200, 150, 100, 70, 50, 30, 10 mb). Data are on a T42 grid and their characteristics have been described by Trenberth (1992). Trenberth (1991) examined how well these analyses satisfy the equation of continuity and concluded that although 14 levels is superior for diagnostic studies, the initialized analyses contain much less noise and much more closely satisfy the mass balance. However, the four-times daily analyses better capture the diurnal cycle.

Methodology

Energy equations

The methodology is related to that used in several other studies but with some important differences. The intent is to obtain the diabatic heating in the atmosphere and use the observed top-of-the-atmosphere radiative fluxes to deduce the flux of heat through the bottom of the atmosphere. One such method uses the apparent heat source Q_1 and apparent moisture sink Q_2 arising

from the thermodynamic and moisture equations (e.g., Yanai et al. 1973, 1976, 1992; Fortelius and Holopainen 1990). The term "apparent" is used because Q_1 and Q_2 include contributions from unresolved eddies. Other methods use the full energy equations in one form or another (e.g., Boer 1982, 1986; Boer and Sargent 1985). In fact there are several options available and, with perfect data, all should be equivalent. In practice, however, large differences arise from the differing formulations because of assumptions made about the data, such as the equation of continuity being satisfied, and it is desirable to explicitly spell out those assumptions to help understand the results and devise the best practical method for obtaining such estimates with minimal contamination from flaws in the data.

Although we have performed diagnostic calculations of the heat and moisture budgets at all levels in the atmosphere, parallel calculations of the mass budget reveal that mass is not conserved by the analyses (Trenberth 1991) and this lack of conservation constitutes a major error component in the other budgets. We have now devised variational approaches to adjust the analyses so that mass is conserved in three dimensions (which will be reported on elsewhere), but the simplest approach and the one pursued here, is to make the corrections and computations through the vertically integrated energy budget as given by Trenberth (1991).

Energy in the atmosphere is usually considered in the form of kinetic energy k, internal energy $I=c_v T$, and potential energy P_e, (e.g., see Boer 1982). The vertical integral of P_e, for example, will be indicated as $\tilde{P}_e$, and is given by

$$\tilde{P}_e = \int_0^\infty g z \rho dz = \frac{1}{g}\int_o^{p_s} (RT+\Phi_s)\, dp$$

after integrating by parts and using the equation of state and hydrostatic equation, and where Φ_s, the surface geopotential, is not a function of pressure.

The thermodynamic equation can be written as

$$c_p\left[\frac{\partial T}{\partial t} + \mathbf{v}\cdot\nabla T + \omega\left(\frac{\partial T}{\partial p} - k\frac{T}{p}\right)\right] = Q_1 \qquad (1)$$

where Q_1 is the diabatic heating. Strictly speaking, k, R, and c_p vary with the amount of moisture in the atmospheric but it is a good approximation to treat them as constant for our purposes. Using the hydrostatic equation, the equation of continuity and the kinetic energy k equation gives

$$\frac{\partial}{\partial t}(c_p T+k) + \nabla\cdot(s+k)\mathbf{v} + \frac{\partial}{\partial p}(s+k)\,\omega = Q_1 + Q_f \qquad (2)$$

where $s=c_p T+\Phi$ is the dry static energy and Q_f is the frictional heating. The latter is small and will be neglected. It is readily shown from (2) after some manipulation involving vertical integrals and properly accounting for the variability of p_s that $E=I+k+P_e$ when integrated over the entire mass of the atmosphere is conserved in the absence of heating and friction.

The moisture conservation expressed in flux form as a heating is

$$L\left(\frac{\partial q}{\partial t} + \nabla\cdot q\mathbf{v} + \frac{\partial}{\partial p} q\,\omega\right) = L(e-c) = -Q_2. \qquad (3)$$

where e is the rate of re-evaporation of cloud and rainwater and c is the rate of condensation per unit mass, which together produce the precipitation rate, the role of liquid water in the atmosphere is ignored, and Q_2 is the latent heat released through evaporation and condensation (Yanai et al. 1973).

Combining Eqs. (2) and (3), gives an expression for the total atmospheric energy transport

$$\frac{\partial}{\partial t}(c_p T+k+Lq) + \nabla\cdot(h+k)\mathbf{v} + \frac{\partial}{\partial p}(h+k)\,\omega = Q_1 - Q_2 \qquad (4)$$

where $h=s+Lq$ is the moist static energy.

The vertical integral through the atmospheric column of Q_1 allows the heating to be broken up into components

$$\tilde{Q}_1 = R_T - R_s + H_s + LP + \tilde{Q}_f \qquad (5)$$

where R_T and R_s are the net downwards radiation through the top of atmosphere and the earth's surface, H_s is the sensible heat flux through the surface, and P is the precipitation rate. Ignoring $\tilde{Q}_f$, then

$$\tilde{Q}_1 = R_T + L(P-E) + F_s \qquad (6)$$

where E is the surface evapotranspiration and

$$F_s = LE + H_s - R_s \qquad (7)$$

is the net upwards flux through the surface. As $\tilde{Q}_2 = L(P-E)$

$$\tilde{Q}_1 - \tilde{Q}_2 = R_T + F_s. \qquad (8)$$

Vertically integrating Eq. (4) through the atmospheric column, and taking the $\frac{\partial}{\partial t}$ and divergence operators outside the integral while accounting for the variability of p_s, gives

$$\frac{\partial}{\partial t}\frac{1}{g}\int_o^{p_s}(c_p T+k+Lq+\Phi_s)\,dp + \nabla\cdot\frac{1}{g}\int_o^{p_s}(h+k)\mathbf{v}\,dp = R_T + F_s. \qquad (9)$$

The first term in Eq. (9) is the change in storage in the atmosphere of internal, potential, kinetic, and latent energy, the second term is the total atmospheric heat transport divergence. In Vonder Haar and Oort (1973) and Oort and Vonder Haar (1976) the k term is dropped from Eq. (9). On an annual mean basis, the changes in storage terms are small and often negligible, so that Eq. (9) may be written as

$$\nabla\cdot\mathbf{F}_A = R_T + F_s \qquad (10)$$

where $\mathbf{F}_A = \frac{1}{g}\int_o^{p_s}(h+k)\mathbf{v}\,dp$ is the atmospheric energy transport. Over land F_s should be close to zero so

$$\nabla \cdot \mathbf{F}_{\mathrm{A}}^{\mathrm{land}} = R_T \tag{11}$$

and the balance lies between the atmospheric energy divergence and the net top-of-the-atmosphere radiation. Within the ocean

$$\nabla \cdot \mathbf{F}_O = -F_s \tag{12}$$

where $\mathbf{F}_O$ is the vertically integrated divergent ocean heat flux.

In using atmospheric data to evaluate Q_1 from Eqs. (1) or (2) it is important to realize the characteristics and shortcomings of the data. If fields are analyzed univariately, as is commonly the case using rawinsonde data, there is no guarantee that the hydrostatic equation is satisfied and other dynamical constraints, such as the winds being close to geostrophic balance, can be grossly violated (Trenberth 1987). However, in that approach the ω field is derived so that the equation of continuity is satisfied. Moreover, it is possible to introduce some dynamical contraints (Savijärvi 1988). The global analyses from operational centers resulting from four dimensional data assimilation have different characteristics. For instance, in the pressure-level archive from ECMWF, the fields are interpolated from model levels and neither the hydrostatic equation nor mass conservation are exactly satisfied in the analyses (Trenberth 1991). The equation of continuity, in particular, can contain residuals exceeding 50% of either term. As a consequence there is no equivalence between Q_1 from Eqs. (1) versus (2) when evaluated from the analyses (see also Ponater and Frenzen 1987).

An attraction to using Eqs. (9) or (10) is the apparent absence of the difficult-to-calculate terms. However, the fluxes are critically dependent on the divergent wind. Consequently, there appear to be considerable advantages to using the advective forms of the equations as in Eq. (1), as they avoid the problems with imbalances in the continuity equation and are much less critically dependent on $\nabla \cdot \mathbf{v}$ being correct. Instead problems come from the ω terms and results depend critically on the reasonableness of ω. Because Eq. (10) is vertically integrated, it is easily corrected for any overall mass imbalance that exists using methods given in Trenberth (1991), whereas this is much more difficult to do using Eq. (1) where decisions about the vertical structure of corrections and how to adjust ω have to be faced.

Another advantage of Eq. (10) is that given estimates of R_T from satellite measurements and using computed values for terms on the left hand side, then F_s can be estimated as a residual. Over the oceans, Eq. (12) then allows estimates to be made of the ocean heat transport. Moreover F_s can be compared with independent estimates made using bulk flux formulations of the surface fluxes.

Most commonly, this approach has not been followed locally and instead Eqs. (10) and (12) have been zonally averaged to obtain total meridional ocean heat transport as residuals (Vonder Haar and Oort 1973; Oort and Vonder Haar 1976; Trenberth 1979; Masuda 1988; Carissimo et al. 1985; Savijärvi 1988; Michaud and Derome 1991). This assumes that Eq. (11) holds and nearly all studies have made this assumption. In fact, it is clear that Eq. (11) is often violated by several tens of W m^{-2} (e.g., this is implied by the results of Fortelius and Holopainen 1990). Firstly, the spurious residual from Eq. (11) may indicate how well this method is actually performing. Secondly, the implication is that some of the "ocean" transport is occurring over land. If, instead, we insist that Eq. (11) holds and then compute the zonal mean ocean transport, rather different results ensue. Alternatively, we can solve for the horizontal heat transport locally and then insist that it should be zero over land. This gives yet another result for the zonal mean. More properly, Eq. (12) should be solved for the ocean region only with appropriate boundary conditions, and this is done here. It is therefore desirable to examine F_s and $\mathbf{F}_O$ regionally much more carefully and critically than has generally been the case in the past.

Practical aspects

We define an overbar to be a finite time average and a prime to denote the departure from that mean, so that, for instance, $u = \bar{u} + u'$. Thus $\bar{u} = \frac{1}{N} \sum_{i=1}^{N} u_i$ where there are N individual values u_i in the mean. Accordingly, when time averages are taken, the energy fluxes may be divided into stationary and transient components of dry static energy s, moist latent energy Lq and kinetic energy k

$$\overline{\nabla \cdot \mathbf{v}(h+k)} = \nabla \cdot \bar{\mathbf{v}}(\bar{s} + L\bar{q} + \bar{k}) + \nabla \cdot \overline{\mathbf{v}'(s' + Lq' + k')}. \tag{13}$$

and the same applies to the corresponding vertical integrals.

We take the means to correspond to monthly means and the transients correspond to departures from the monthly means. The atmospheric terms, including the tendency terms, have been evaluated for each month and the yearly mean is computed from the average of the individual monthly means. The tendency term is small.

The mass weighted vertical integral of any quantity M

$$I = \int_{p_t}^{p_s} M\,dp/g \tag{14a}$$

can be written as

$$I = \frac{1}{g} \int_{p_t}^{p_o} \beta M\,dp \tag{14b}$$

where p_o is now some fixed value of pressure greater than p_s everywhere, and we define $\beta = 0$, $p > p_s$; $\beta = 1$, $p \le p_s$. This has the potential advantage of having fixed integration limits (e.g., Boer 1982).

Because data are available only at fixed pressure levels, Eq. (14) must be replaced with finite differences. In each case, the vertical integral will be carried out using a trapezoidal rule. We set $p_o = 1100$ mb say,

and $p_{2J}=p_t$. Then for Eq. (14b) we define the layer thickness $\Delta p_j=p_{j-1}-p_{j+1}$, $j=1,3,\ldots 2J-1$. With these definitions, the trapezoidal rule of integration is exactly equivalent to

$$I=\frac{1}{g}\sum_{j=1,2J-1,2}(\beta M)_j\Delta p_j \tag{15}$$

and we define

$$\begin{aligned}\beta_j&=1 \quad \text{if} \quad p_{j-1}<p_s\\ \beta_j&=0 \quad \text{if} \quad p_{j+1}>p_s\\ \beta_j&=\frac{p_s-p_{j+1}}{p_{j-1}-p_{j+1}} \quad \text{if} \quad p_{j-1}>p_s>p_{j+1}\end{aligned} \tag{16}$$

so that $0\le\beta\le 1$. This is more accurate than the definitions used for β by Boer (1982).

This approach correctly weights the values at each level in the vertical with the appropriate mass of the layer and gives exact results in the case where M is a constant, for example. Note, however, that because of the missing data in the stratosphere in the seven level case, we will generally prefer to use $p_t=50$ mb rather than zero as the upper limit for integration.

Generally we have found by changing the number of p-levels used that for any A, the $\frac{\partial A}{\partial p}$ terms are better evaluated in finite difference form in lnp coordinates as $\frac{1}{p}\frac{\delta A}{\delta lnp}$ using centered differences where possible.

If lnp is chosen for the vertical coordinate, an equivalent set of expressions to Eqs. (13) to (16) exists except then the vertical integral in Eq. (14) becomes

$$\int_0^{p_s} M\frac{dp}{g}=\int_0^{lnp_s} pM\frac{dlnp}{g}=\frac{1}{g}\int_{lnp_t}^{lnp_o} p\beta M\,\mathrm{d}\ln p.$$

Then Eqs. (15) and (16) must also be appropriately modified to correspond to the new coordinate.

Several approaches were tried in properly dealing with the lower boundary and the p_s values. The latter were computed for the real world orography (Trenberth 1992) and were also available from ECMWF for the analyses on the artificial model surface which corresponds to an enhanced envelope orography, often with p_s values lower by 50 to 100 mb or more in the vicinity of complex high mountains (Trenberth 1992). On p-levels, therefore, values as archived are extrapolated below the envelope orography as part of the post processing at ECMWF. There is no "correct" way to do this and our experience indicates that all such values are somewhat contaminated. It is therefore necessary to use the ECMWF p_s values and neglect that part of the real atmosphere below the artificial surface. Moreover, we have found that it is also desirable to ensure that no part of the extrapolated values enters into the calculations or else extremely noisy fields result in the vicinity of mountains. Therefore, in all cases, the lowest layer was treated very conservatively and sometimes omitted. This practical difficulty in obtaining reasonable results near complex terrain is a compelling reason why it may be better to carry out diagnostic analyses in model coordinates, but interpolating from p to model coordinates only compounds the problems, so it is necessary to obtain the original model-level data. For the present diagnostics, however, it means that results cannot be considered accurate near mountains and this aspect will make results over land less reliable than over the oceans.

Most results presented here are for the 7-level initialized ECMWF analyses. Later we comment on results using other datasets. All calculations were performed at T42 resolution but results have generally been truncated to T31 resolution for presentation purposes. On the vector plots (Figs. 4–9) only every second gridpoint vector is shown.

Top-of-the-atmosphere radiation

Comprehensive analyses of the earth radiation budget using satellite data have been presented in the past, for instance Stephens et al. (1981) summarized results from all measurements prior to 1980. Hartmann et al. (1986) summarized shortcomings in radiation budget data at that time and noted the presence of unacceptably large uncertainties in top-of-the-atmosphere radiation data for use in the heat budget, but that the ERBE was expected to substantially reduce those uncertainties. In particular, ERBE has had an objective of improving measurements of the diurnal variations in the radiation budget so that more accurate radiation products can be derived. This has been achieved by using three satellites (ERBS, NOAA 9 and NOAA 10) carrying identical instrument packages. Barkstrom et al. (1989) made estimates of the uncertainties in ERBE scanner data on a monthly mean regional basis as about ± 5 W m^{-2} for both the shortwave and longwave radiation. Global-mean average-annual radiation was also estimated to have uncertainties of ± 5 W m^{-2}. More comprehensive error estimates were made by Rieland and Raschke (1991). Average root mean square (rms) sampling errors due to diurnal sampling for outgoing longwave radiation (OLR), absorbed solar radiation (ASR), and net radiation were 0.9, 3.4 and 3.5 W m^{-2} respectively for the three satellites combined. However, these numbers increase to about 3, 8 and 9 W m^{-2} for just one satellite. In addition, when other uncertainties from data inversion procedures are included, the final ERBE rms uncertainty estimates are 7.8 W m^{-2} for the three satellite combination versus 11 W m^{-2} for one satellite.

Use is made of the ERBE data for the year 1988, by which time NOAA 9 had failed. [As the NOAA 10 scanner failed in May 1989, it is not practicable to use more recent data unless major compromises are made in sampling, or non-scanner data are substituted (which is not recommended by the ERBE science team). The ERBS scanner failed in February 1990.] Overall rms error estimates are ± 9 W m^{-2} for two satellites, with larger errors coming from the ASR than OLR. Because the global mean net radiation averaged

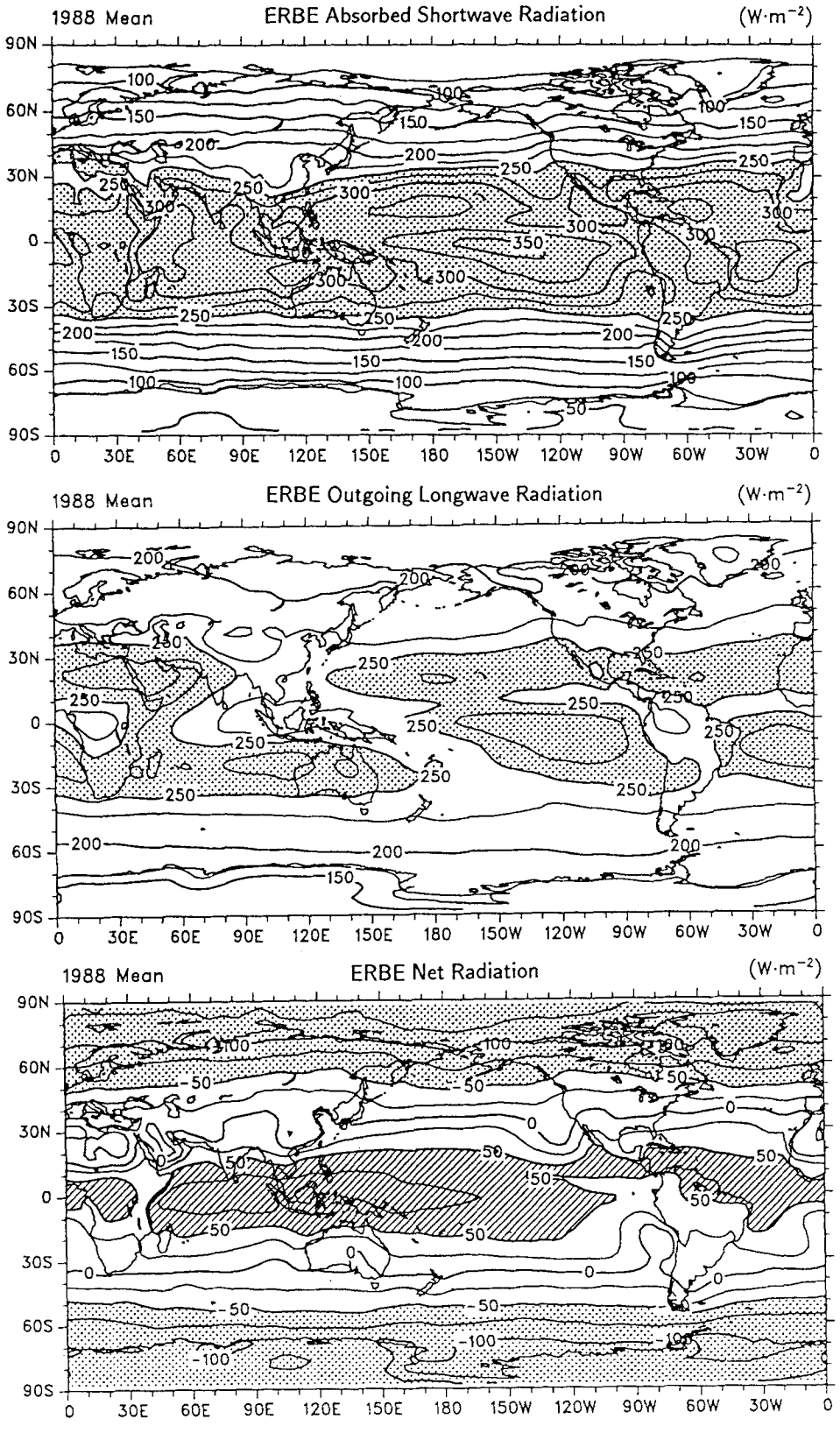

Fig. 2. Mean top-of-the-atmosphere radiation from ERBE for 1988 in W m^{-2}. Shown are the absorbed shortwave radiation (ASR), the outgoing longwave radiation (OLR), and the net R_T. Values greater than 250 W m^{-2} are *stippled* in the *top two panels*, and values exceeding ± 50 W m^{-2} are either *stippled* or *hatched* in the *bottom panel*

over one year does not integrate to zero, corrections need to be applied to remove this bias. The global mean value may, of course, depart slightly from zero if there is a change in heat stored by the Earth system, but this is believed to be ~ 1 W m^{-2} at most. Standard deviations of global net radiation from Nimbus 7 are 0.5 W m^{-2} (Ardanuy et al. 1962). As the main uncertainty in the net radiation arises from the ASR, we have made a slight adjustment to the ERBE-derived albedo in order to achieve a global annual balance in

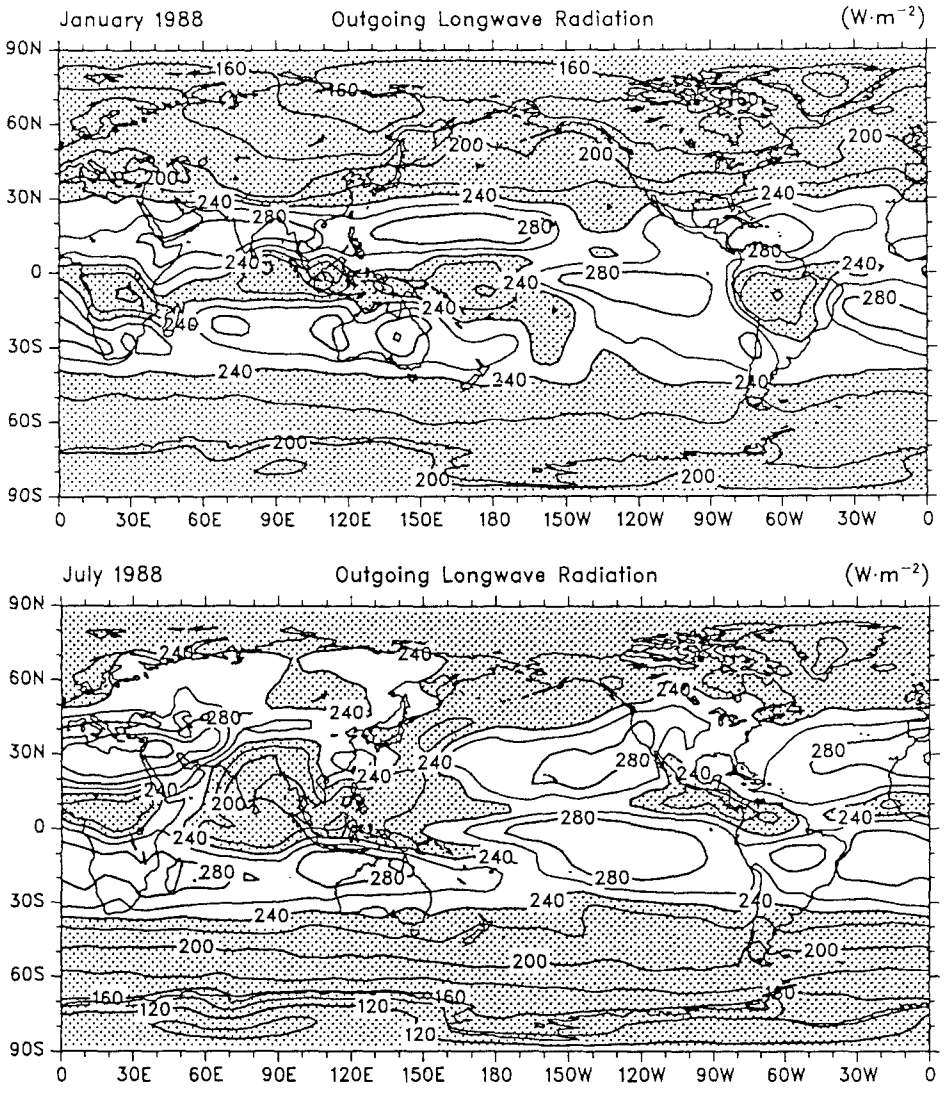

Fig. 3. Outgoing longwave radiation from ERBE in W m^{-2}, for January and July 1988. Values less than 240 W m^{-2} are *stippled* and indicate regions of convection (high cloud tops) in the tropics

radiation. Thus, the correction is not uniform in net radiation over the globe as has typically been the case in past studies, but is weighted by the solar radiation distribution. For 1988, the global imbalance is 4.1 W m^{-2}.

Figure 1 shows the zonal mean ASR and OLR with the difference, which constitutes the net radiation, highlighted by shading. It reveals the excess of ASR over OLR in the tropics and the deficit at high latitudes. The spatial patterns of the 1988 annual mean ASR, OLR and net radiation are presented in Fig. 2. OLR in the tropics is dominated by the presence or otherwise of high cold cloud tops, and is often used as an index of convection. Thus values less than 250 W m^{-2} show the main annual mean convergence zones and these can also be seen in the ASR as regions of higher albedo. Features are qualitatively similar to those from previous studies but the small quantitative regional differences that are present from previous studies, arising in part because this is for a specific year, are important in the current context.

The year 1988 featured strong circulation anomalies associated with the end of the 1986–87 El Niño-Southern Oscillation (ENSO) event, which ended by March 1988, and the very strong 1988 La Niña event that developed in April and May 1988, and persisted throughout the rest of the year. In January 1988, tropical Pacific SSTs were above normal and convection was displaced eastward along the equator to the vicinity of the dateline. By July, SSTs were substantially below normal along the equator and the dry zone along the equator was enhanced although above normal activity occurred in the South Pacific Convergence Zone (SPCZ) (Trenberth and Branstator 1992). These aspects are revealed by the OLR for January and July 1988 in Fig. 3 and should be kept in mind in interpreting the maps presented later for these two months.

Atmospheric heat transports

The atmospheric heat transports have been broken up into rotational and divergent parts, and also into time mean "stationary" and transient components. The rotational transports are the nondivergent part and, although much larger than the divergent component, are

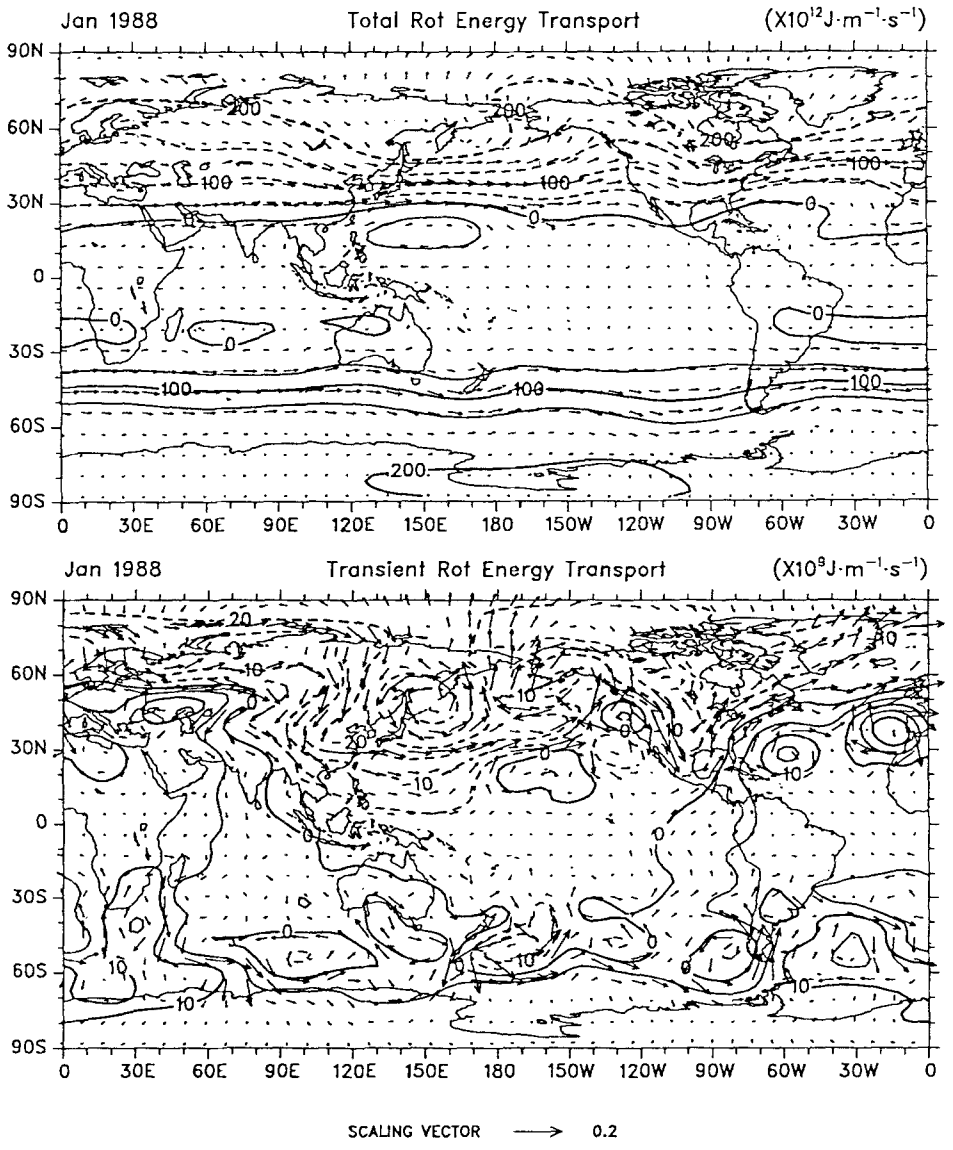

Fig. 4. Rotational component of the total and transient total energy flux for January 1988. For the mean, the scaling vector is 0.2×10^{12} J m^{-1} s^{-1} and the streamfunction is in 10^{15} J s^{-1}, while for the transient component the scaling vector is 0.2×10^{9} J m^{-1} s^{-1} and the streamfunction is in 10^{13} J s^{-1}

not tied to the sources and sinks of energy (Boer and Sargent 1985; Boer 1986). The contributions from the dry static energy, latent energy and kinetic energy have been evaluated for each month of the year. It is not possible to show all of these here but it is useful to show the dominant contributions for January and July to illustrate the most important terms and mechanisms, and their seasonal variation.

Figures 4 and 5 show for January and July the rotational component of the energy transport for the total and transient contributions in the form of vectors and the stream-function. Their difference is the contribution from the stationary component but, as the latter is two orders of magnitude larger than the transient component, it looks very like the total field. The rotational transports are dominated by the contribution from the rotational part of the wind (Boer and Sargent 1985) and the results given here, while quite similar to those of Boer and Sargent for 1979, also reflect the interannual variations noted above.

The divergent kinetic energy transport is an order of magnitude less than any other component and will not be shown. Also, as the time mean component dominates the transient component, so that it looks somewhat like the total field, it will not be presented.

Figures 6 and 7 show the total and transient components of the divergent energy transports for January 1988 and Figs. 8 and 9 show the same for July 1988. The three panels in each figure correspond to the total energy, the dry static energy, and the latent energy, where the total includes the kinetic energy component. The zonally integrated transports are given in Fig. 10. Although the transient component is smaller than the stationary component, it is quite significant, especially in midlatitudes and it becomes relatively much more important in the zonal integral. Boer and Sargent (1985) and Boer (1986) have previously presented similar results for the dry static energy for 1979.

In January, the transient poleward fluxes (Fig. 7) are strong in both hemispheres and the dry static ener-

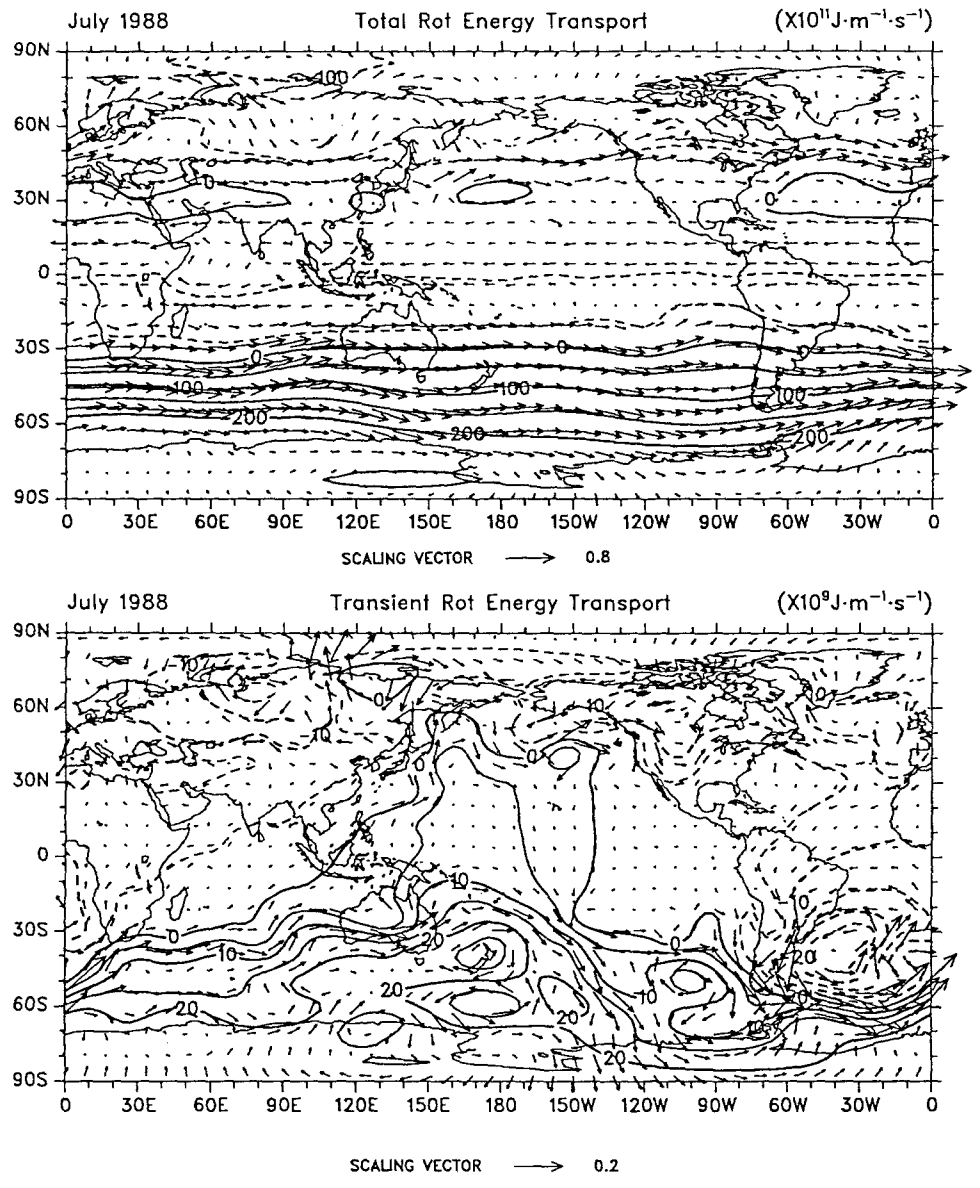

Fig. 5. Rotational component of the total and transient total energy flux for July 1988. The scaling vector is 0.8×10^{11} J m^{-1} s^{-1} and the streamfunction is in 10^{15} J s^{-1}, while for the transient component the scaling vector is 0.2×10^{9} J m^{-1} s^{-1} and the streamfunction is in 10^{13} J s^{-1}

gy component is roughly double that of the latent energy. The latter is also true in July (Fig. 9), but the NH transports are much weaker than in the SH and in January. For the mean and total fields (Figs. 6, 8), it is noticeable that part of the energy flux in the tropics in the form of dry static energy is cancelled by the latent component. This occurs as the convergence of moisture in the low levels is realized as latent heating, so that the net total transport is somewhat less than that for dry static energy alone in the tropics. In fact, any inconsistency between the moisture and heat transports in the tropics which should result in strong cancellation between these two terms means that errors in the small residual can be large.

While part of the mean transport occurs as a stationary wave transport in the NH in January, most comes from the large-scale overturning in the atmosphere associated with the divergent wind component as manifest in the Hadley and Walker circulations. Note the strong seasonal global-scale monsoon changes from January to July in Figs. 6 and 8. The dominant energy outflow center coincides closely with the region of highest SSTs in the oceans. The anomalous convection in the tropical Pacific (Fig. 3) has its signature in Fig. 6 as well. The zonally symmetric Hadley component is clearer in the dry static energy panel of these figures but with dominant contributions from the eastern hemisphere. The east-west outflow is best seen across the Pacific. However, it is clear that the zonal and meridional outflows are combined and any depiction with Hadley and Walker-type breakdowns is an oversimplification.

It is the divergent part of the flow and its associated transport which is most uncertain and which has changed quantitatively with time, e.g., since 1979 (see Boer and Sargent 1985). Trenberth (1992) shows how the zonal mean Hadley circulation has changed at ECMWF with the changes in the data assimilation system. Consequently, the transports shown in Figs. 6–10 are improved and substantively different than in pre-

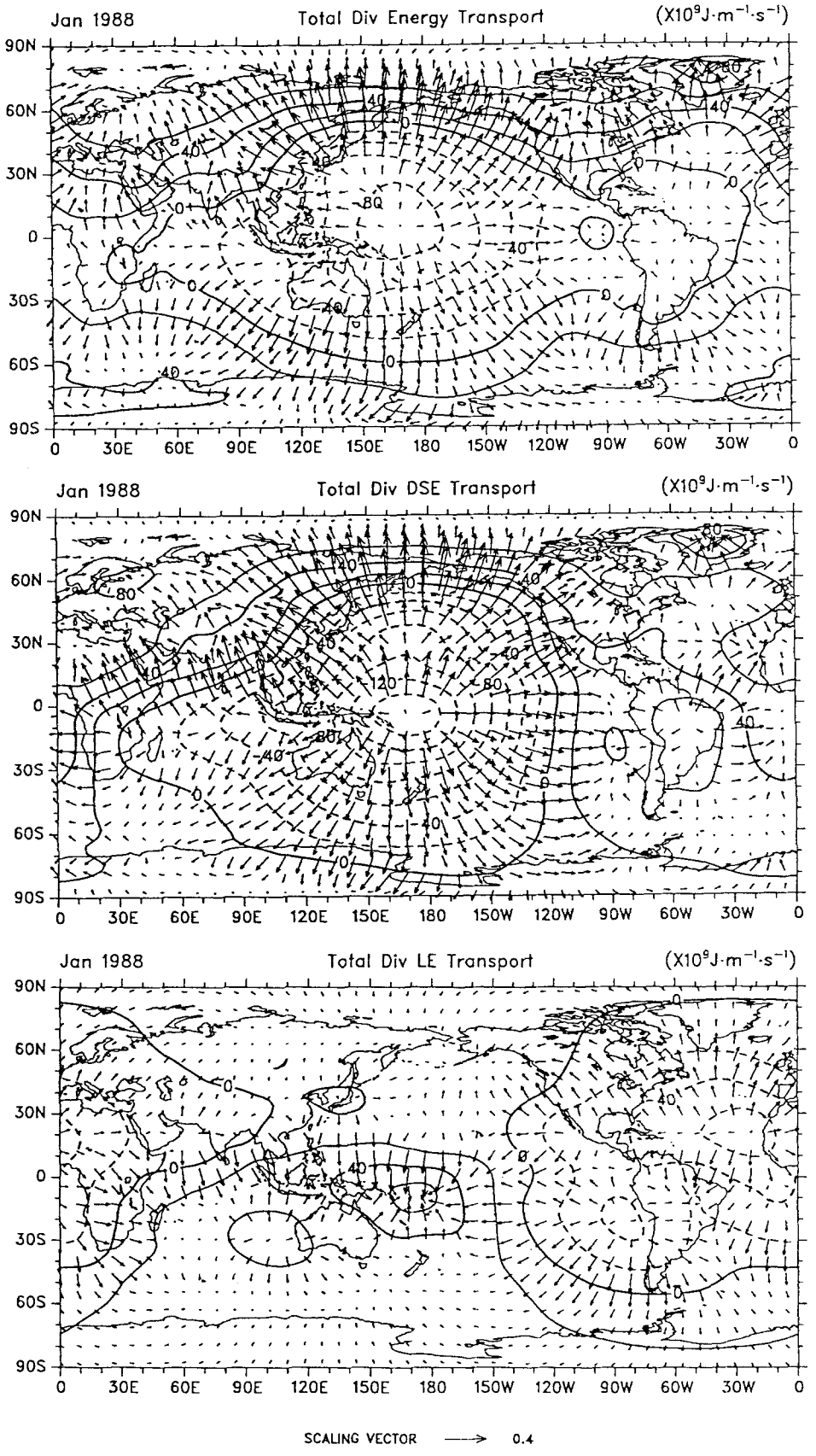

Fig. 6. Total (stationary plus transient) divergent energy transport component for the total, dry static, and latent energy components for January 1988. The scaling vector is 0.4×10^9 J m^{-1} s^{-1} and the potential function is in 10^{13} J s^{-1}

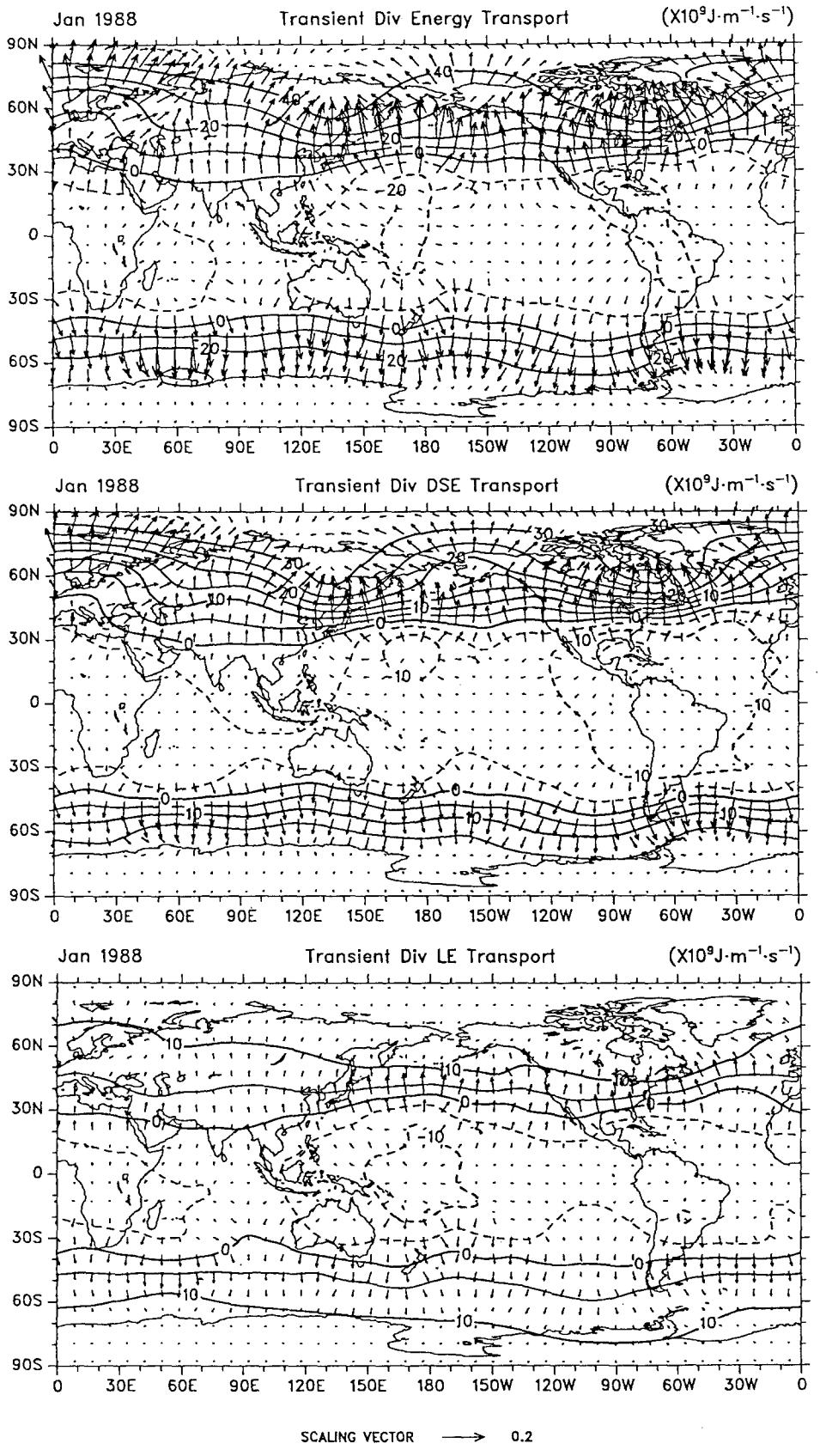

Fig. 7. Transient divergent energy transport component for the total, dry static, and latent energy components for January 1988. The scaling vector is 0.2×10^9 J m^{-1} s^{-1} and the potential function is in 10^{13} J s^{-1}

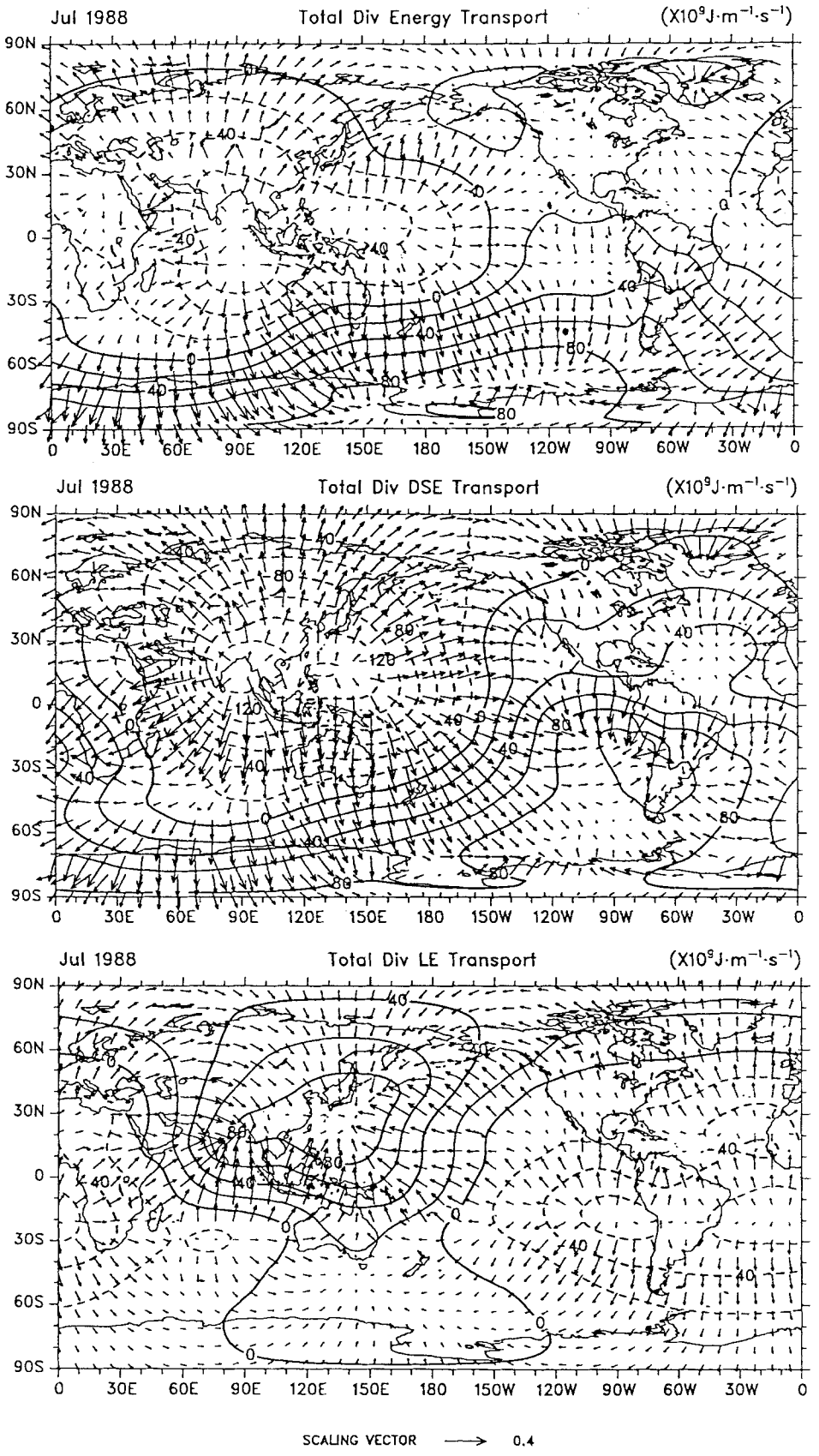

Fig. 8. Total (stationary plus transient) divergent energy transport component for the total, dry static, and latent energy components for July 1988. The scaling vector is 0.4×10^9 J m^{-1} s^{-1} and the potential function is in 10^{13} J s^{-1}

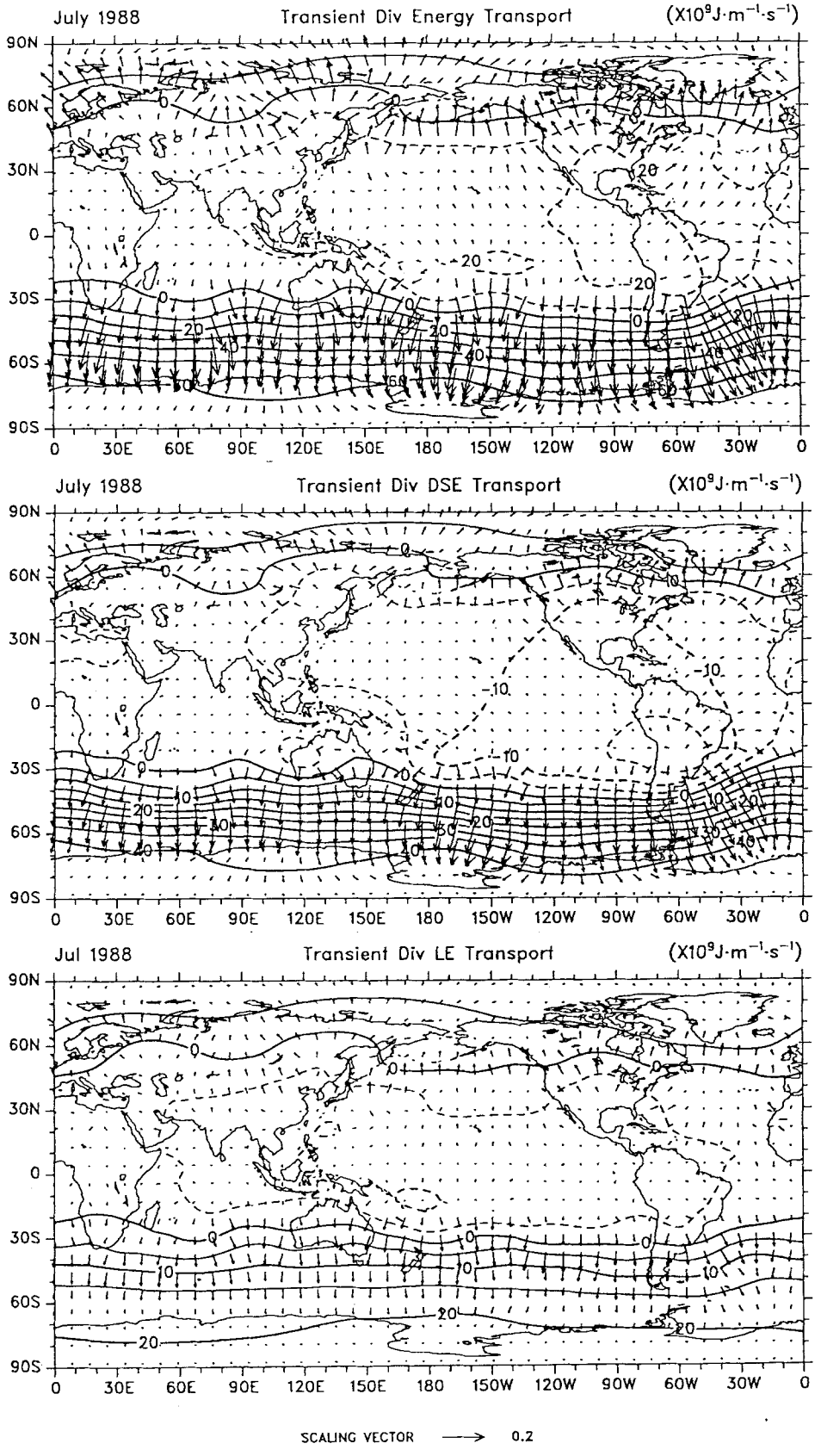

Fig. 9. Transient divergent energy transport component for the total, dry static, and latent energy components for July 1988. The scaling vector is 0.2×10^9 J m^{-1} s^{-1} and the potential function is in 10^{13} J s^{-1}

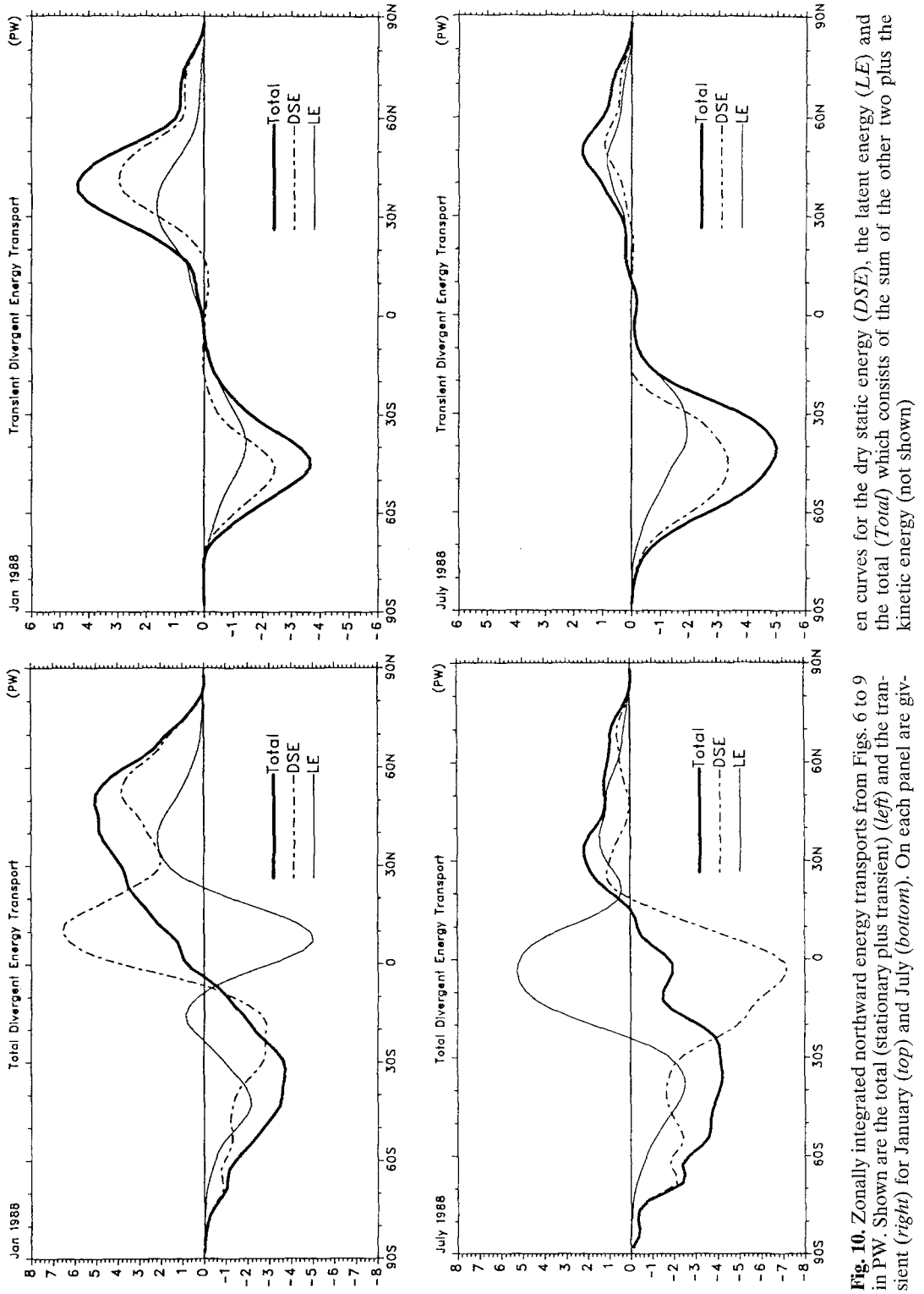

Fig. 10. Zonally integrated northward energy transports from Figs. 6 to 9 in PW. Shown are the total (stationary plus transient) (*left*) and the transient (*right*) for January (*top*) and July (*bottom*). On each panel are given curves for the dry static energy (*DSE*), the latent energy (*LE*) and the total (*Total*) which consists of the sum of the other two plus the kinetic energy (not shown)

vious studies, especially those based on rawinsonde observations such as Savijärvi (1988). However, further improvements are desirable, as discussed later.

Derived atmospheric heating

The picture seen in Figs. 6 and 8 reveals the dominance of the tropical western Pacific in January and southeast Asia in July as a major heat source for the atmosphere. The corresponding $\tilde{Q}_1$ and $-\tilde{Q}_2$ fields from Eqs. (2) and (3), expressed as part of (9) in vertically integrated form, are given in Figs. 11 and 12 for both January and July. In both figures the ITCZs over the Pacific and Atlantic, the SPCZ and the monsoonal convection over tropical continental land can be clearly seen in both the moisture convergence as given by $\tilde{Q}_2$ and diabatic heating as given by $\tilde{Q}_1$. These features agree

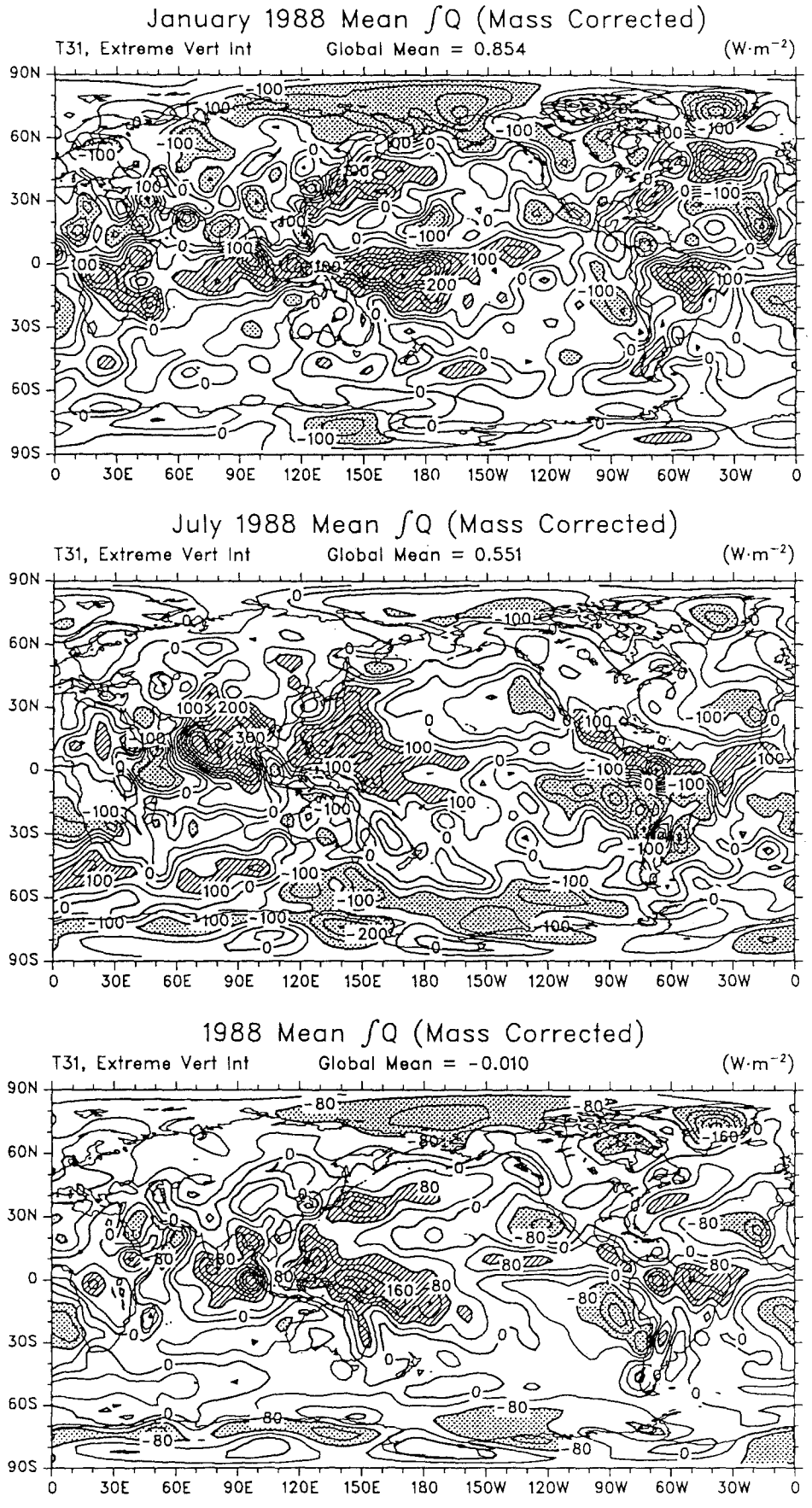

Fig. 11. $\tilde{Q}_1$ for January and July 1988 and the annual mean in W m^{-2}. The contour interval is 50 W m^{-2} on the *top two panels* and 40 W m^{-2} on the *bottom*

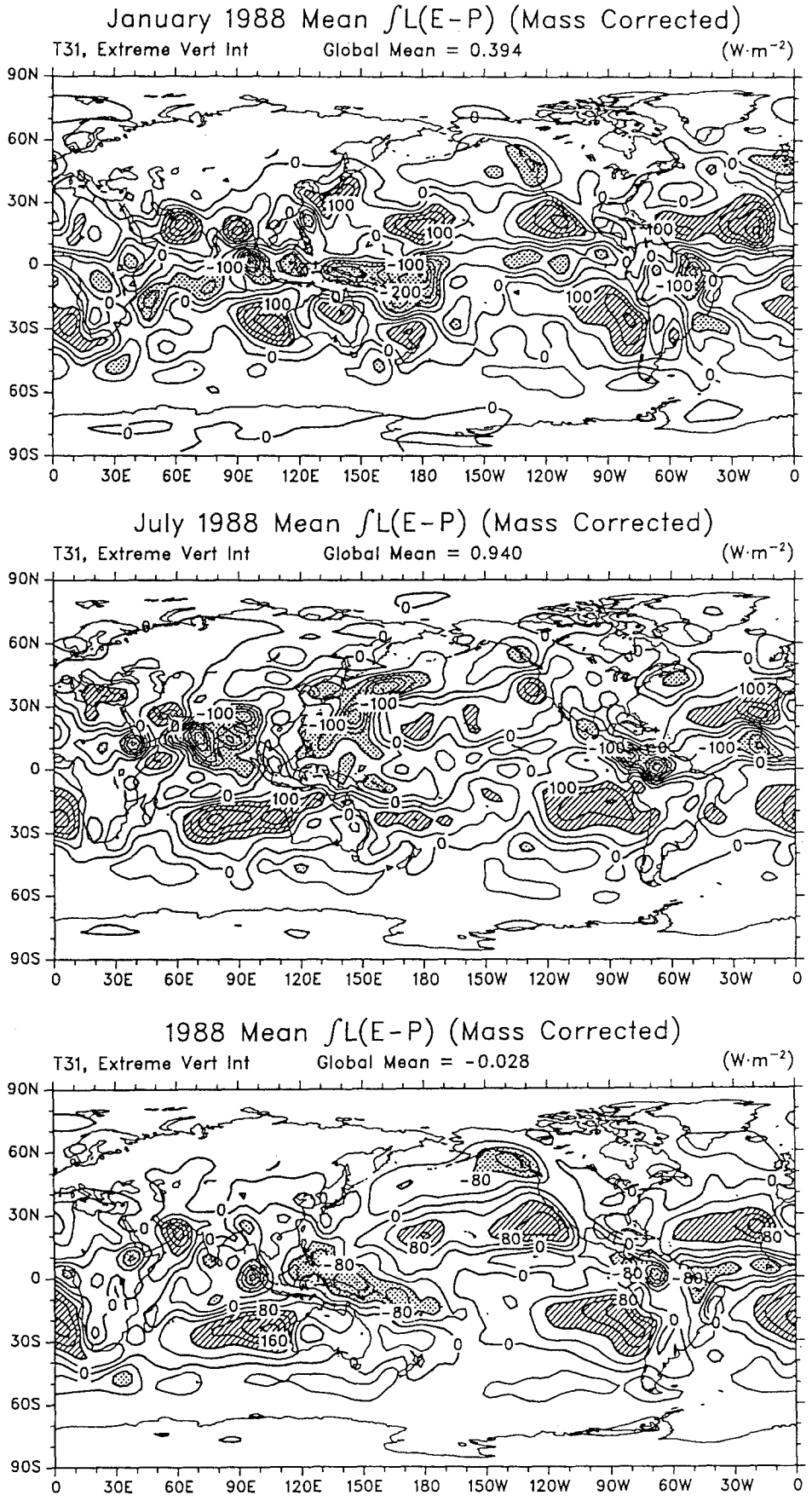

Fig. 12. $-\tilde{Q}_2 = L(E-P)$ for January and July 1988 and the annual mean in W m^{-2}. The contour interval is 50 W m^{-2} on the *top two panels* and 40 W m^{-2} on the *bottom*

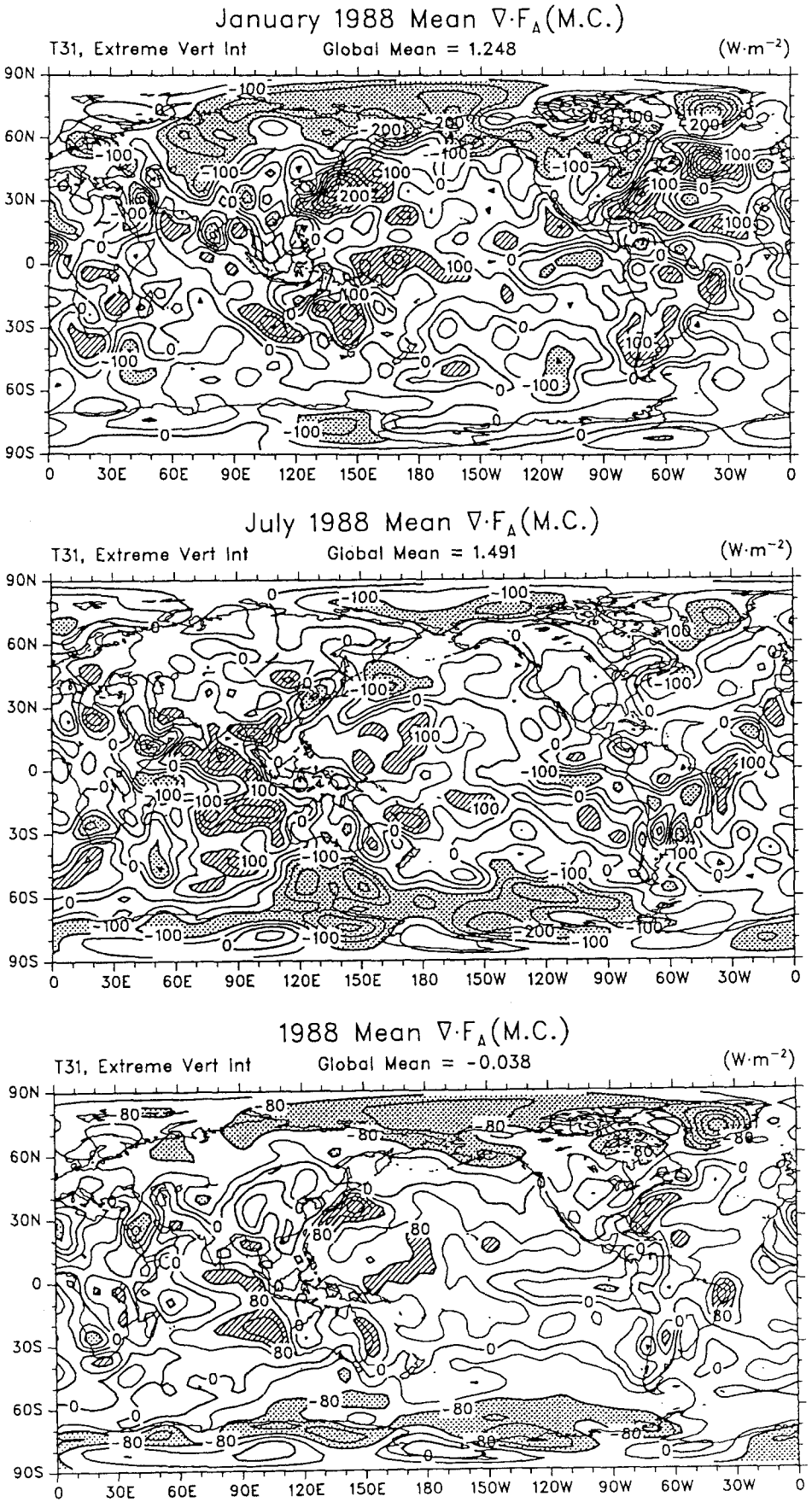

Fig. 13. The divergence of the atmospheric energy transport $\nabla \cdot \mathbf{F}_A$ for January and July 1988 and annual mean in W m^{-2}. The contour interval is 50 W m^{-2} on the *top two panels* and 40 W m^{-2} on the *bottom*

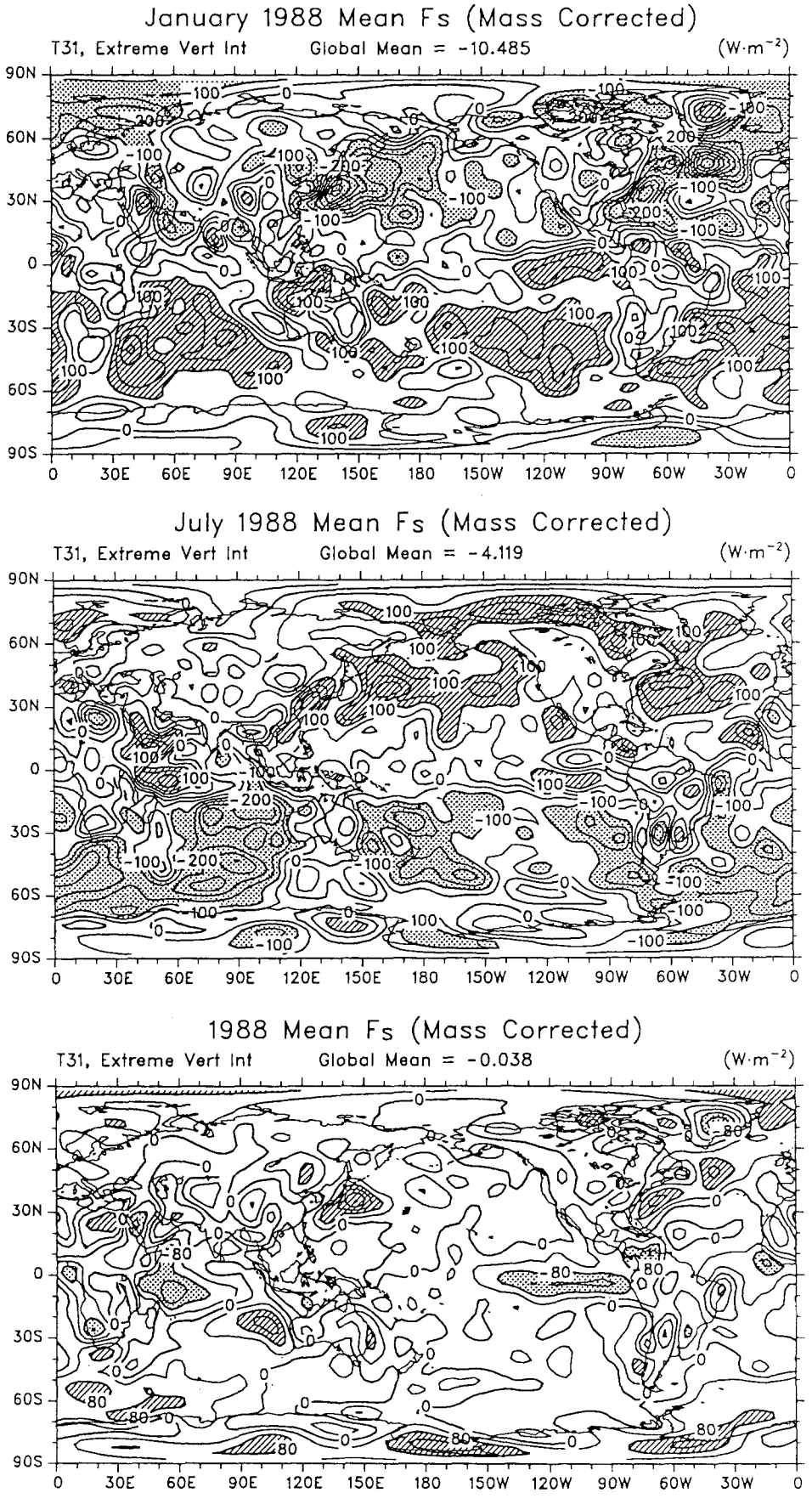

Fig. 14. The net surface energy flux F_s for January and July 1988 and annual mean in W m^{-2}. The contour interval is 50 W m^{-2} on the *top two panels* and 40 W m^{-2} on the *bottom*

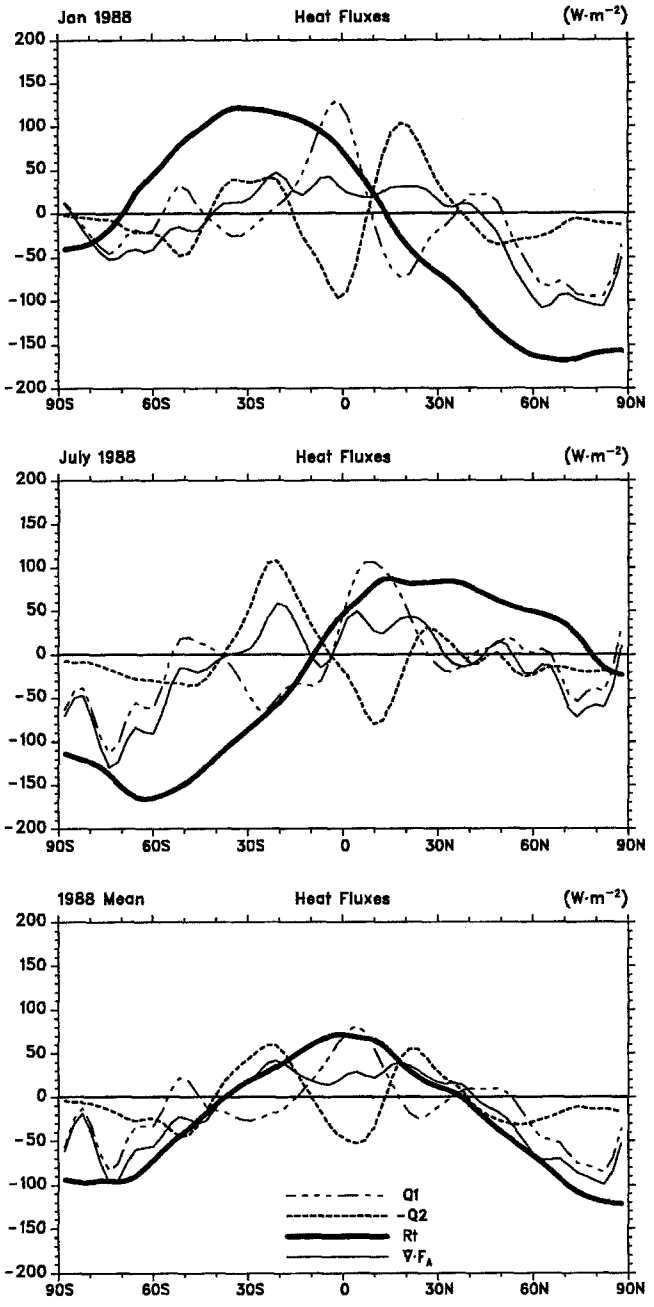

Fig. 15. Zonal means of R_T, $\tilde{Q}_1$, $-\tilde{Q}_2$, and $\nabla \cdot \mathbf{F}_A$ for January and July 1988 and annual mean in W m^{-2}

quite well with those deduced from OLR (Fig. 3) in the tropics although there are differences in detail.

The combination of Figs. 11 and 12 as $\tilde{Q}_1 - \tilde{Q}_2$ (see Eqs. 4–9) is equivalent to the divergence of the atmospheric energy transport (see Eq. 10), and is given in Fig. 13. In January, NH extratropical features over the western parts of the oceans, which were also present in Fig. 11, emerge as dominant features. These large heat source regions for the atmosphere are from cold dry continental air moving over the relatively warm ocean with consequential large sensible and latent heat fluxes into the atmosphere. In July the largest heat source for the atmosphere is from evaporation over the subtropical Indian Ocean. The sources of strong latent heating in the tropics are still in evidence but seem a bit weak, perhaps indicating too much cancellation between $\tilde{Q}_1$ and $\tilde{Q}_2$. This would be the case if the large-scale divergent flow is too weak in 1988 and, as discussed later, this is probably the case.

When the fields in Fig. 13 are combined with R_T for January and July (see Fig. 15 for zonal means) the net flux through the surface of the atmosphere is obtained (see Eq. 10), and the results are given in Fig. 14. In January, when the net radiative heating is nearly all south of 10°N, the ocean is generally cooling over the NH with strong heat fluxes into the atmosphere, and the reverse is true in July. The changes in heat storage are not negligible for these months. However, the annual mean results over the oceans can be interpreted through Eq. (12) as the heat sources and sinks for the ocean that are not manifested as changes in heat storage and thus as the divergence of the vertically integrated ocean heat transport.

Zonal averages of several of these fields for January, July and the 1988 mean are given in Fig. 15 and for July they can be compared with those from 1979 (Boer 1986). The strong cancellation between $\tilde{Q}_1$ and $\tilde{Q}_2$ is especially evident in these plots. The strong seasonality of the top-of-the-atmosphere radiation and the more subdued change in the divergence of the atmospheric transports is apparent.

One commentary on the quality of the these derived fields comes from the physical constraints over land. For $\tilde{Q}_1$ these are addressed in the next section. For $\tilde{Q}_2$ on an annual mean basis, changes in moisture storage over land are small so that $P > E$ in order to account for the runoff in rivers. In Fig. 12 therefore, the values should be negative over land. Notable exceptions to this occur over South America and Australia, and a few other more isolated spots.

The net surface flux can be compared with results from bulk flux methods over the oceans, such as from Hsiung (1985) and Oberhuber (1988), and Isemer and Hasse (1987) for the North Atlantic, among others. Qualitatively the results are similar, with the regions of strong fluxes into the atmosphere off the east coast of the northern continents in January and in the annual mean, and with heat fluxes into the ocean in the summer hemisphere and in the equatorial regions on an annual mean basis. Quantitatively the results differ, but it is uncertain as to how much this is due to the fact that our results are for 1988, not a long-term average. Thus in January, for instance, Oberhuber (1988) and Isemer and Hasse (1987) indicate a maximum flux into the atmosphere near 35°N off the coast of North America exceeding 400 W m^{-2} while the current results indicate a 300 W m^{-2} contour. Instead, in January 1988, values exceed 500 W m^{-2} in the North Atlantic near 50°N. Values exceed 400 W m^{-2} in both Fig. 14 and Oberhuber's climatology near Japan in January. In the annual mean, results from Hsiung (1985) and Oberhuber (1988) agree with present estimates of a net flux into the ocean exceeding 100 W m^{-2} in the equatorial east Pacific. The overall pattern of a strong ocean heat source in a fairly narrow zone in all three

tropical oceans and with the main ocean heat sinks off the east coasts of the northern continents is robust in all studies.

The magnitude of the heat sink for the ocean in the subtropical Indian Ocean near 30°S is much stronger in Fig. 14 than in Hsiung and Oberhuber's results and while both of these studies reveal a similar heat sink in the Pacific it is surprisingly absent in Fig. 14. It is expected that the oceans around Antarctica should be a heat source for the atmosphere in much the same way as the ocean is off the east coasts of North America and Asia, as cold dry air outbreaks interact with the open ocean, but this shows up only in the southern Indian and Atlantic Ocean sectors. Results over the Southern Ocean in the Pacific sector do not seem credible for these reasons, probably because it is the region of the globe with the fewest in situ observations. These shortcomings will be manifested in the computed ocean transports unless adjusted for.

Ocean heat transports

As noted in the Introduction, the conventional way to compute the ocean transports using the residual method has been to take the zonal mean of the radiatively required poleward heat flux and the atmospheric transports, and subtract, assuming that the result gives the ocean transports (Fig. 16). But implicit in this approach is the assumption that the "ocean transports" are zero where there is land. Inevitably this is not true. As we noted in discussing Eq. (11), over land there should be a balance between R_T and the atmospheric heat divergence. This balance is measured by the results in Fig. 14 over land where F_s should be close to zero for the mean annual cycle. Clearly it is not. Values over land are typically $\pm 30\ \mathrm{W\,m^{-2}}$ and sometimes exceed $100\ \mathrm{W\,m^{-2}}$. The problems in F_s over Greenland, the Andes and Antarctica have been reduced by the use of the conservative procedures in the vertical integral described in the third section. Nevertheless, even in the eastern North America and Australia where high mountains are not a factor and the data base is very good, the residuals are not small.

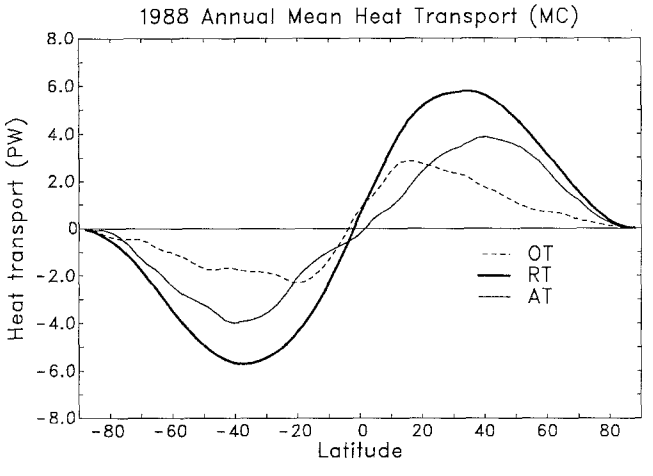

Fig. 16. The top-of-the-atmosphere required northward heat transport from satellite radiation measurements RT, the estimated atmospheric transports AT, and the ocean transports OT computed as a residual, for 1988 in PW

The patterns of F_s over the oceans are larger in scale. Also, because F_s is computed from the divergence of the atmospheric transports, it is unlikely to have systematic errors except for the tropical regions. The systematic global bias in R_T has been removed. Accordingly, using the land results averaged over regions of 1000 km square, we estimate empirically that the values over the oceans may have a standard error of $\sim 30\ \mathrm{W\,m^{-2}}$ over these scales. We use this as a means of setting error bars on the ocean transports. It is very difficult to assign realistic error bars, and traditional error analysis has always greatly underestimated the true error bars (as seen, for example, by the absence of overlap among error bars from different estimates). Here we use an ad hoc procedure but one that is realistic and which scales linearly with the local standard error. It therefore provides an estimate of how the errors accumulate over certain areas.

As noted, one answer for the zonal mean poleward ocean heat transports is the difference between the radiatively required and atmospheric transports (Fig. 16). If instead we set $F_s = 0$ over land as it should be, and solve Eq. (12) for the ocean transports by taking only zonal means, then a different answer emerges. Equation (12) can also be solved locally with F_s as computed or set to zero over land, then ignoring the land contribution to the fluxes gives two more answers. But none of these solutions can be considered correct, and they give quite different results from the correct solution. The correct method is to solve Eq. (12) with proper boundary conditions that fully recognize the distribution of land and that there is no heat flux normal to the coastline. By setting up a potential field for the divergent ocean heat transport $\mathbf{F}_O = \nabla\chi$ and using F_s as a forcing function, we are required to solve a Poisson equation $\nabla^2\chi = -F_s$ subject to the boundary conditions that the heat flux through the continental boundaries must be zero ($\nabla\chi \cdot \mathbf{n} = 0$). This equation imposes another constraint because the mean over the domain of integration of F_s must then be zero. Thus, an integral constraint on F_s is not simply that the global mean must be zero, but also that the value over land should be zero and the mean over the oceans should be zero. Unless adjusted in some way, this is not the case for the field in Fig. 14.

To obtain a better understanding of this aspect of the problem, we have first simplified the problem by taking zonal means of Eq. (12) across each ocean basin and integrated southwards under the assumption that the F_s values are probably better over the more densely observed northern oceans. Firstly a simplified land-ocean mask was devised. At 65°N there is a minimum in ocean available for northward heat transport and estimates are that the transport through the Bering Strait is 0.2×10^{13} W, and in the North Atlantic 1.4×10^{14} W (Aagaard and Greisman 1975). Also, at 70°S, $\mathbf{F}_O \to 0$

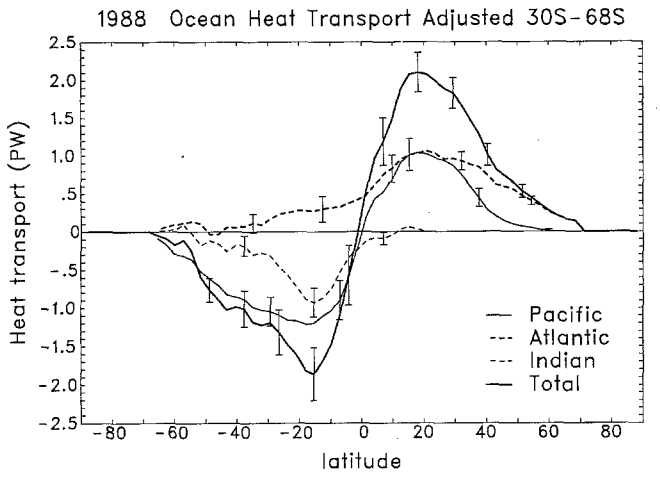

Fig. 17. The poleward ocean heat transports in each ocean basin and summed over all oceans (*total*), as computed from the net flux through the ocean surface, integrated from 65°N and adjusted south of 30°S, for 1988 in PW. As this calculation does not account for the Indonesian throughflow, the Pacific and Indian ocean contributions should be combined

(all land/ice). In the Indian Ocean the northward ocean heat flux is zero at the northern boundary. Using these values specified as the northern boundary condition, we then integrate

$$OT = \bar{\mathbf{F}}_{O_y} = -\int \bar{F}_s a \, d\phi$$

for each ocean basin, where $\bar{\mathbf{F}}_{O_y}$ is the zonally integrated northward ocean flux and $\bar{F}_s$ is the zonal integral in longitude across the basin of F_s. The integral is carried out in finite difference form using Gaussian quadrature.

Using this method and integrating the unadjusted F_s values to 68°S gives a northward heat flux at 68°S of 0.4 PW in the Atlantic, 0.1 PW in the Indian and −1.2 PW in the Pacific oceans. This highlights the problems we noted earlier as having an insufficient flux out of the ocean in the Pacific, in particular. To satisfy the Southern Ocean heat flux constraint, we have required that the ocean heat transport should go to zero at 68°S, and to achieve this the simplest method is to adjust the ocean heat fluxes south of 30°S linearly with latitude. The result is shown in Fig. 17.

When a similar correction is applied to the F_s field itself, and the entire Eq. (12) is solved for the potential function subject to boundary conditions that there is no heat flux through the ocean boundaries, using an iterative technique, the result is given in Fig. 18. The correction guarantees that the integral of the surface flux over the global ocean domain is zero, as it must be to solve the Poisson equation. In interpreting this figure, it must be recalled that it gives only the divergent heat flux component. An additional rotational component is not available from this method. Thus over the southern oceans, the heat carried eastwards in the Antarctic Circumpolar Current is not represented and nor is any gyre transport. The results south of 30°S cannot be trusted.

As noted earlier, in Fig. 17 error bars are assigned representing plus or minus one standard error in the

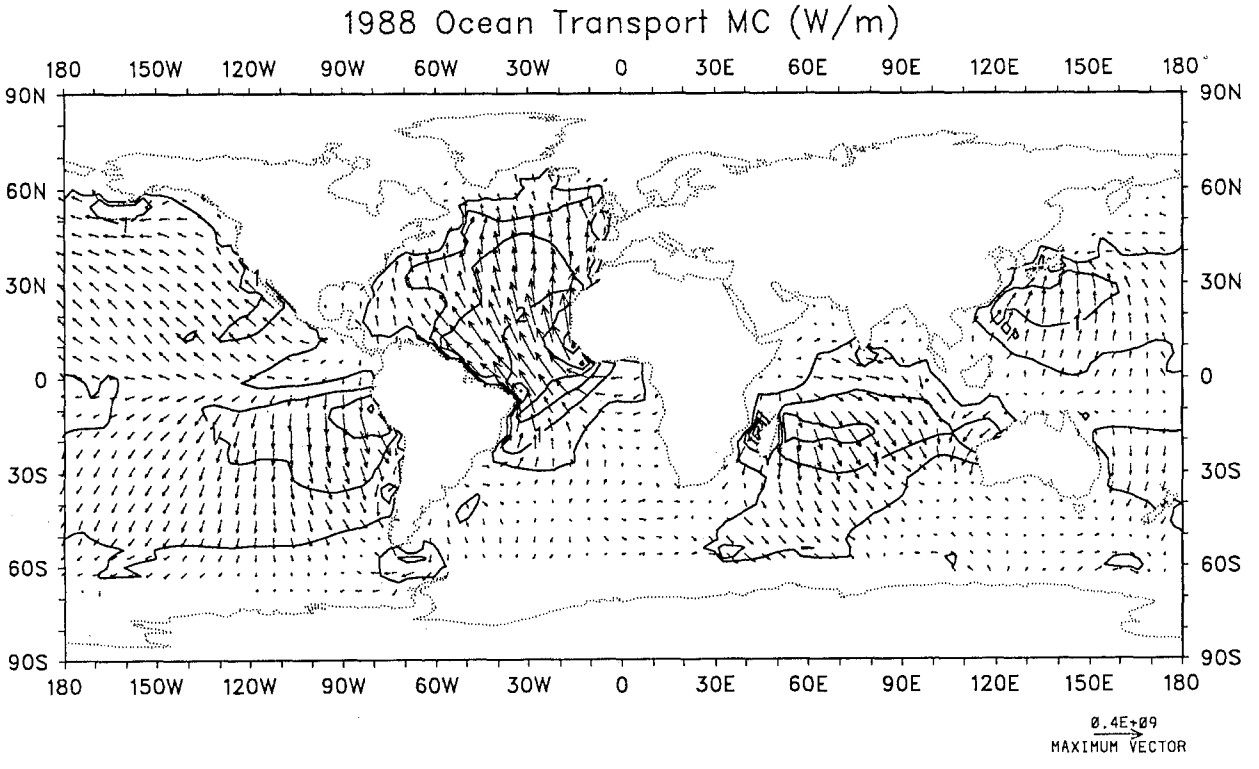

Fig. 18. The vectors of divergent ocean heat transport for 1988 from solving Eq. (12). The simplified coastal outlines are indicated. Units are 10^8 W m^{-1} and the vector for 4×10^8 W m^{-2} is indicated at *lower right*. The contours indicate the magnitude of the vectors

mean transport within each ocean and for the total based on assumed random errors of 30 W m^{-2} over 1000 km scales. Consequently, the error is related to the area of each ocean relative to the high latitude boundary in both hemispheres.

In spite of the reservations about the calculations discussed the results are of interest both in terms of their overall magnitudes and the patterns of the heat fluxes so revealed. In the Atlantic, a northward transport emerges at all latitudes with peak values of 1.1 ± 0.2 PW at 20 to 30°N. Comparable values are achieved in the Pacific at 20°N, so that the total is 2.1 ± 0.3 PW. The peak poleward transport at 15 to 20°S of -1.9 ± 0.3 PW is made up of strong components from both the Pacific and Indian Oceans. Note that the interpretation of these basin contributions is ambiguous because, in reality, there is a throughflow from the Pacific into the Indian Ocean which means that there is a net northward mass flux in the Pacific, at say 30°S, and a net southward mass flux at the same latitude in the Indian Ocean. This mass flux transports heat which is not accounted for in Fig. 17, so that it is only the sum of the two ocean contributions that is meaningful.

The regional pattern of the inferred ocean heat fluxes (Fig. 18) is also of interest. The pattern of poleward ocean heat fluxes in low latitudes is suggestive of a strong role for Ekman transport of warm surface water which returns colder at some depth. This is especially so in the Pacific and Indian oceans, but also in the Atlantic, although it is masked there by the overall northward heat flux component that is evidently associated with the large-scale thermohaline circulation. The pattern elsewhere is harder to interpret and it is noticeable that there is no clear signature from the boundary currents. Nor is it obvious that there should be because the rotational heat fluxes are not included here. For instance, the superposition of a rotational subtropical gyre transport in the North Atlantic would partly cancel the divergent component over the eastern part of the ocean while reinforcing the poleward transport in the western boundary current. In the Indonesian area, a heat flux from the Pacific into the Indian Ocean is apparent, although it has its source in the western tropical Pacific.

Discussion and conclusions

New estimates of the net top-of-the-atmosphere radiation from ERBE have allowed improved estimates of the required heat transports by the atmosphere and ocean. Moreover, we have used improved estimates of the global atmospheric heat transports from recent ECMWF analyses. Together these allow updated estimates of the ocean heat transports as a residual. Unlike many previous studies, however, we have performed the heat budget locally and with data for the same period, which allows a more complete evaluation of the results. Although there are still errors in the radiation measurements of significance, the estimate is that the errors bars are ± 9 W m^{-2} and with the overall annual mean for 1988 of 4.1 W m^{-2} as a measure of the systematic bias for 1988. However, the uncertainties in the various components of the atmospheric transports, although difficult to quantify, probably dwarf these numbers.

Atmospheric transports

For the atmospheric transports, the largest problems are believed to lie in the two areas of (1) large-scale atmospheric divergence and (2) the moisture budget, although several other factors are also of note. These are discussed in turn next.

1. Problems with atmospheric divergence. In low latitudes the estimates of atmospheric divergence and the associated large-scale overturning in the Hadley and Walker circulations were especially poor in earlier rawinsonde-based analyses but have been improving steadily in global analyses. A history of the changes in the ECMWF analyses is given by Trenberth (1992) who shows that a major strengthening of the Hadley cell occurred following the May 2, 1989 changes in the ECMWF data assimilation system and the model used. In July 1988, the mass flux in the Hadley circulation was 210×10^9 kg s^{-1} but this increased to over 280×10^9 kg s^{-1} in 1989, 1990 and 1991 (Trenberth 1992) although even within those years its character (e.g., size and location of center in the vertical) changed. In January, the Hadley circulation mass flux also increased from about 200 to about 250 units.

An examination of the performance of the ECMWF model before and after the change on May 2, 1989 with regard to whether the precipitation is "spinning up" or "spinning down" is given in Trenberth (1992). The evidence suggests before the May 1989 change that both precipitation and evaporation were too low initially and rapidly spun up, whereas following the May 1989 change, there was a large overestimate of precipitation at time 0 in JJA 1989, although with more reasonable values the following DJF and with evaporation still required to spin up. The implication appears to be that the analyzed ω in the tropics may be somewhat weak from May 1985 to May 1989, and thus the atmospheric poleward heat transports underestimated.

Overall, the analyzed strength of the Hadley Cell has increased since 1988, the year of our analysis, by 25 to 35%. The implication is that increases have occurred in the poleward heat transports in the tropics. However, because there is strong cancellation between the Q_1 and Q_2 contributions, the net effect on the total heat budget is somewhat ameliorated. Calculations by Keith (1994) indicate the net effect of the change on the low latitude total heat transport is ~10%. Sardeshmukh (1993) has shown the inconsistency of the "analyzed" divergence field with the vorticity budget and that it was too weak for the period 1982 to 1985, in particular. Sardeshmukh and Liebmann (1993) have

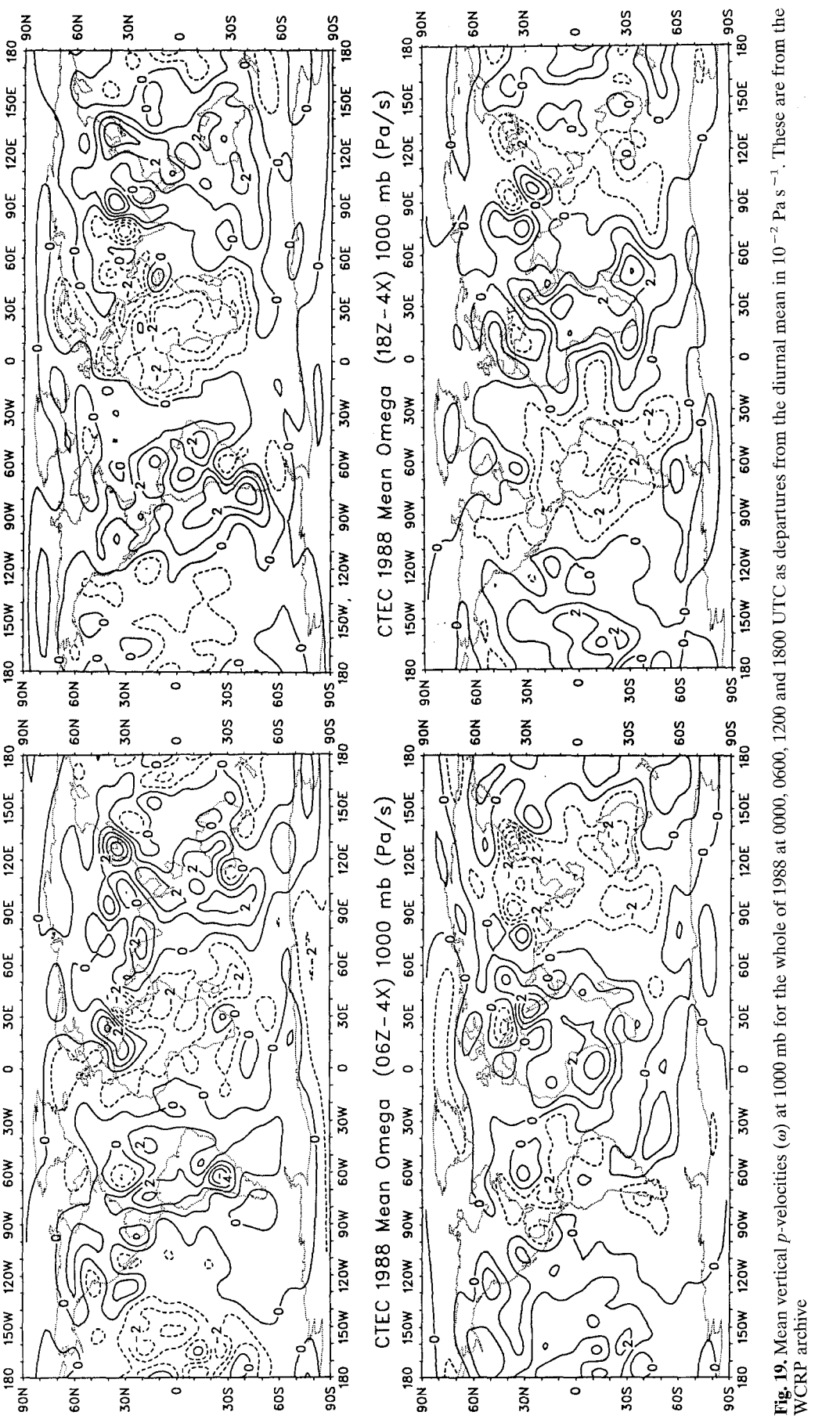

Fig. 19. Mean vertical p-velocities (ω) at 1000 mb for the whole of 1988 at 0000, 0600, 1200 and 1800 UTC as departures from the diurnal mean in 10^{-2} Pa s^{-1}. These are from the WCRP archive

further demonstrated the inconsistencies between ECMWF and US National Meteorological Center (NMC) divergence fields for 1988 to 1989. While there continue to be large changes in the divergence as analyzed, studies of the momentum and vorticity budgets indicate that there is now a possibility that the Hadley cell may be analyzed to be too strong after May 1989. Diabatic initialization of the analyzed fields imposes a somewhat artificial balance that may overstrengthen zonal mean meridional circulations (Errico and Rasch 1988; Errico 1991). Nevertheless, there has been a clear improvement with time in the tropical analyses although problems remain (Errico 1991).

2. The diurnal cycle. Previous studies have not resolved the diurnal cycle and use has been of once or twice-daily analyses. The same has been true here because the only four-times per day analyses available to us are uninitialized (see point 4 later). However, four-times-daily analyses mostly capture the diurnal cycle. To show how large this is in the analyses, we have computed the mean vertical motions at several levels for all months for 1988 at 0000, 0600, 1200 and 1800 UTC, and the daily mean. The departures of each time from the daily mean for the whole of 1988 are given in Fig. 19 at 1000 mb. The diurnal cycle is more striking in the low atmosphere where there is a large component from the semidiurnal and diurnal tides (Trenberth 1991). At 0000 UTC the sun is over 180°E/W, at 0600, 1200 and 1800 UTC the sun is over 90°E, 0° and 90°W, respectively. Thus, in Fig. 19 it can be seen that coherent large-scale upward motions are maximized about 20° longitude behind the sun and a weaker upward maximum occurs 180° out of phase. The strong wave two structure associated with the semidiurnal tide is clearly evident. The same wave one and wave two patterns are evident at 500 mb, but there is considerably more smaller scale noise also present; the magnitudes are about the same. A major part of the diurnal cycle and its semidiurnal component is probably real, however, almost certainly part of it arises from the fact that observations are taken mostly at 0000 and 1200 UTC and in many places only once per day, so that spurious components are no doubt introduced by the distribution of observations. Because of the semidiurnal component, analyses twice daily contain a strong residual diurnal cycle component. Therefore, none of the atmospheric budgets, and in particular the mass and heat budgets, can be considered adequately determined until the diurnal cycle is fully incorporated. If the diurnal cycle does not affect the heat budget, then the effects can be mostly removed by correcting the mass budget (see point 3).

3. Mass imbalances remain in all analyses. Mass imbalances are quite large and will totally distort other budgets unless corrected for. Fortunately, to first order this is relatively straightforward to do (Trenberth 1991) and this correction also removes most of the problems with not adequately resolving the diurnal cycle. However, the correction is to the vertical integral and does not take account of the vertical distribution of the correction.

4. Initialized versus uninitialized analyses. The mass imbalance problem mentioned in (3) is much worse in the uninitialized analyses (Trenberth 1991). Vertical motions and divergence fields tend to be stronger but noisier in the uninitialized analyses and this led us to reject them for the current analysis.

5. Vertical resolution. The current analysis was based on only 7 levels in the vertical. Improved vertical resolution is important although our calculations show that the differences are relatively small compared with the other items mentioned already. In particular, improved resolution is needed in the boundary layer for the moisture budget, and in the boundary layer and upper troposphere for divergence.

6. Interpolation to p surfaces. The archives of global atmospheric analyses are generally made available in p coordinates. The archival postprocessing of interpolating from model coordinates, on which the analyses are performed, to p levels introduces errors (Trenberth 1991) and results, for instance, in the equation of continuity no longer being satisfied. Earlier (section three), we also discussed the difficulty in properly dealing with the lower boundary of the atmosphere in p coordinates. Discrepancies exist between the true surface of the Earth and that depicted in the global analyses, and problems are apparent near mountains. Even so, it may be worthwhile using model coordinates for future diagnostic analyses, although these too are not without substantial difficulties. In addition to the problem of surface depiction, the process of changing resolution (e.g., from T106 to T42) to facilitate processing large amounts of data is ill defined in model coordinates (Trenberth et al. 1993).

7. Moisture budget. We earlier noted the problems with the results over land where it is not physically possible for E to be greater than P for an annual mean. This is one indication of remaining difficulties with the moisture budget which is very likely linked to points 5 and 6 above.

As well as making diagnostic computations with the ECMWF analyses, we are also carrying out similar calculations using the NMC analyses. Trenberth and Olson (1988) reported on earlier comparisons for analyses prior to 1987. At present, in depth comparison of more recent analyses from 1988 through 1992 has been carried out for the moisture budget. Over regions of good data, such as North America, the agreement in these budgets is quite good. But over the oceans, the disagreements are large, and locally are almost the same order as the terms themselves. We find discrepancies in the tropics in $L(E-P)$ for the zonal means of 20 to 30 W m^{-2}, or the root mean square zonal mean discrepancies are $\sim$90 W m^{-2} (or for $E-P \sim 3$ mm/day) compared with rms values of 120 W m^{-2}. These discrepancies are present throughout the 1987 to

1992 period and, if anything, get slightly larger with time. The results will be reported on elsewhere. Fortunately, the uncertainties in the total heat budget are much less because of the cancellation between Q_1 and Q_2 as the moisture convergence is realized as latent heating.

8. Residual surface fluxes. It is not clear how well the overall local heat budget is known, however, the results from Fig. 14 over land indicate that the uncertainty is of the order of ± 30 W m^{-2} on scales of 1000 km or so, where this should be regarded as a standard error. In Fig. 17 we used these estimates to provide error bars for the poleward ocean transports. These error bars will be too low in low latitudes because of the biases noted already.

Ocean transports

As noted, one complication in assessing the ocean transports arises from connections between the oceans, such as that in the Indonesian throughflow, which means the meridional heat transports are meaningful only if the Pacific and Indian oceans are combined.

MacDonald (1993) summarizes previous literature on the Indonesian throughflow and suggests the best estimate is 10 Sv (10^9 kg s^{-1}), although Hirst and Godfrey (1993) estimate the throughflow as 16 ± 4 Sv. However, MacDonald notes the considerable uncertainty attached to this estimate and that seasonal and interannual variations may be an important factor. She also surveyed heat transports and used several hydrographic surveys over the oceans at 30°S to estimate the poleward heat transports consistent with a model in which various Indonesian throughflows were used. Her results give a net southward transport of -0.7 PW broken up into 0.3 PW in the Atlantic, and -1.0 PW for the Pacific and Indian combined (-1.3 PW for the Indian, 0.3 PW for the Pacific). Hirst and Godfrey (1993), in a series of model experiments, find the Indonesian throughflow contributes to a southward increase in heat transport in the Indian Ocean and a decrease in the Pacific, with heat transport in the throughflow of 0.63 PW out of the Pacific Ocean. Their total meridional heat transport by the model ocean at 30°S is -2.0 PW. The Fine Resolution Antarctic Model (FRAM) numerical diagnostic experiment (Saunders and Thompson 1993) has a southward heat flux at 30°S of -0.53 PW made up of 0.56, 0.01 and -1.10 PW in the Atlantic, Pacific and Indian Oceans, respectively.

In the NH, Bryden et al. (1991) have estimated heat transports across 24°N using direct oceanographic methods and they find the net northward heat flux by the oceans to be 2.0 PW broken up into 0.76 PW by the Pacific and 1.22 PW in the Atlantic. These results are believed to be the best direct ocean estimates available with error bars of ± 0.3 PW in each ocean or ± 0.45 PW for the total across 45°N (Bryden 1993). The total is remarkably similar to the total ocean transport from this study.

There are considerable uncertainties in these estimates. For instance, the Hellerman and Rosenstein (1983) wind stresses used by Bryden et al. (1991) and in the FRAM study are quite uncertain over the southern oceans and differ considerably from more recent estimates (Trenberth et al. 1990). The wind stresses influence the Ekman transport estimates. Direct ocean measurements do not include annual cycle sampling or interannual variability and both are considerable in the Semtner and Chervin (1988, 1992) model (Chervin, personal communication 1993) and also in the Community Modeling Effort (Bönning and Herrmann 1994). Other biases arise from the methodology (especially assumptions about the width of the boundary currents and the geostrophic assumption).

It is evident from the scatter in the direct ocean observational estimates, the questions arising from methodology and sampling, and in the ocean model results that considerable uncertainty remains in just what is the poleward ocean heat transport from the direct or model oceanographic methods. Given the uncertainties in the atmospheric components, it is also apparent that very large uncertainties exist in the ocean transports computed with residual methods. It is clear that previous estimates, both direct and indirect, have considerably underestimated the error bars (if they were given at all). Nevertheless, several things can be concluded.

1. Local calculations. The calculations of ocean heat transports should not be done solely on the basis of zonal means using residual methods. All, or almost all, previous studies using the residual method have computed ocean poleward heat transports by subtracting the zonal mean atmospheric component from the radiation component, without examining the implied surface fluxes. Large nonzero surface fluxes over land on an annual mean basis are an indication of the accuracy of the method and should be properly accounted for before valid conclusions can be made about the ocean heat transports. Complications from surface topography, however, add considerably to the difficulty of achieving a balance over land. Consequently the heat budgets should be done locally.

2. Ocean heat fluxes. Poleward heat fluxes by oceans in the current study are generally smaller than in previous estimates using residual methods. This is especially the case for previous studies based solely on rawinsonde measurements which fail to capture the vigor of the circulation and atmospheric heat transports over the oceans, and which are even more uncertain in the tropics. For the individual basins, the current results seem more credible and are close to some direct oceanographic estimates. The largest heat sink in the atmosphere proves to be from evaporation over the subtropical Indian Ocean in the SH, resulting in a stronger southward oceanic heat transport in the Indian Ocean that is compatible with results from several other studies that examine the Indonesian throughflow phenomenon (e.g., MacDonald 1993; Hirst and Godfrey 1993).

Results also indicate a stronger poleward transport in both hemispheres in the Pacific than most oceanographic studies. The pattern of poleward ocean heat fluxes (Fig. 18) in low latitudes is suggestive of a strong role for Ekman transport of warm surface water which returns colder at some depth. The pattern elsewhere is harder to interpret, in large part because it reveals only the divergent component. Seasonal variations in ocean models (Bönning and Herrmann 1994) appear to be considerable and add to the difficulty of this interpretation, although the results indicate major contributions from the wind-driven circulation. In the Indonesian area, a heat flux from the Pacific into the Indian Ocean has its source in the western tropical Pacific.

Acknowledgements. Thanks to Chris Guillemot for preparing most of the figures and Frank Bryan for help with the Poisson equation solution. The ECMWF data used were provided by ECMWF. This research is partly sponsored by the Tropical Oceans Global Atmosphere Project Office under grant NA87AANRG0208, and NASA under NASA Order No. W-18077. The National Center for Atmospheric Research is sponsored by the National Science Foundation.

References

Aagaard K, Greisman P (1975) Toward new mass and heat budgets for the Arctic Ocean. J Geophys Res 80:3821–3827

Ardanuy PE, Kyle HL, Hoyt DV (1992) Global relationships among the Earth's radiation budget, cloudiness, volcanic aerosols and surface temperature. J Clim 5:1120–1139

Barkstrom B, Harrison E, Smith G, Green R, Kibler J, Cess R, ERBE Science Team (1989) Earth Radiation Budget Experiment (ERBE) archival and April 1985 results. Bull Am Meteorol Soc 70:1254–1262

Boer GJ (1982) Diagnostic equations in isobaric coordinates. Mon Weather Rev 110:1801–1820

Boer GJ (1986) A comparison of mass and energy budgets from two FGGE datasets and a GCM. Mon Weather Rev 114:885–902

Boer GJ, Sargent NE (1985) Vertically integrated budgets of mass and energy of the globe. J Atmos Sci 42:1592–1613

Bönning CW, Herrmann P (1994) On the annual cycle of poleward heat transport in the ocean: results from high resolution modeling of the North and Equatorial Atlantic. J Phys Oceanogr 24:91–107

Bryden HL (1993) Ocean heat transport across 24°N latitude. In: Interactions between global climate subsystems, the legacy of Hann. Geophys Monogr 75 IUGG 15, IUGG, AGU, pp 65–75

Bryden HL, Roemmich DH, Church JA (1991) Ocean heat transport across 24°N in the Pacific. Deep-Sea Res 38:297–324

Carissimo BC, Oort AH, Vonder Haar TH (1985) Estimating the meridional energy transports in the atmosphere and ocean. J Phys Oceanogr 15:82–91

Dobson FW, Smith SD (1988) Bulk models of solar radiation at sea. Q J R Meteorol Soc 114:165–182

Errico RM (1991) Theory and application of nonlinear normal mode initialization. NCAR Tech Note NCAR/TN-344+IA

Errico RM, Rasch PJ (1988) A comparison of various normal-mode initialization schemes and the inclusion of diabatic processes. Tellus 40A:1–25

Fortelius C, Holopainen EO (1990) Comparison of energy source estimates derived from atmospheric circulation data with satellite measurements of net radiation. J Clim 3:646–660

Hartmann DL, Ramanathan V, Berroir A, Hunt GE (1986) Earth radiation budget data and climate research. Rev Geophys Space Phys 24:439–468

Hastenrath S (1980) Heat budget of tropical ocean and atmosphere. J Phys Oceanogr 10:159–170

Hastenrath S (1982) On meridional heat transport in the world ocean. J Phys Oceanogr 12:922–927

Hellerman S, Rosenstein M (1983) Normal monthly wind stress over the world ocean with error estimates. J Phys Oceanogr 17:1093–1104

Hirst AC, Godfrey JS (1993) The role of Indonesian throughflow in a global ocean GCM. J Phys Oceanogr 23:1057–1085

Hsiung J (1985) Estimates of global oceanic meridional heat transport. J Phys Oceanogr 15:1405–1423

Hurrell JW, Campbell CG (1992) Monthly mean global satellite data sets available in CCM History Tape format. NCAR Tech Note NCAR/TN-371+STR

Isemer H-J, Hasse L (1987) The Bunker climate atlas of the North Atlantic Ocean. Vol 2 air-sea interactions. Springer, Berlin Heidelberg New York, 252 pp

Keith D (1994) Meridional energy transport: uncertainty in zonal means. Tellus (in press)

MacDonald AM (1993) Property fluxes at 30°S and their implications for the Pacific-Indian throughflow and the global heat budget. J Geophys Res 98:6851–6868

Masuda K (1988) Meridional heat transport by the atmosphere and the ocean; analysis of FGGE data. Tellus 40A:285–302

Michaud R, Derome J (1991) On the mean meridional transport of energy in the atmosphere and oceans as derived from six years of ECMWF analyses. Tellus 43A:1–14

Oberhuber JM (1988) An atlas based on the COADS data set: the budgets of heat, buoyancy and turbulent kinetic energy at the surface of the global ocean. Max Planck Institute for Meteorology Rep 15, Max Planck Institute for Meteorology, Hamburg, Germany

Oort AH, Vonder Haar TH (1976) On the observed annual cycle in the ocean-atmosphere heat balance over the Northern Hemisphere. J Phys Oceanogr 6:781–800

Ponater M, Frenzen G (1987) On the numerical evaluation of the energy conversion integral. Tellus 39A:515–520

Rieland M, Raschke E (1991) Diurnal variability of the earth radiation budget: sampling requirements, time integration aspects and error estimates for the Earth Radiation Budget Experiment (ERBE). Theor Appl Climatol 44:9–24

Sardeshmukh PD (1993) The baroclinic χ problem and its application to the diagnosis of atmospheric heating rates. J Atmos Sci 50:1099–1112

Sardeshmukh PD, Liebmann B (1993) An assessment of low-frequency variability in the tropics as indicated by some proxies of tropical convection. J Clim 6:569–575

Saunders PM, Thompson SR (1993) Transport, heat and freshwater fluxes within a diagnostic numerical model (FRAM). J Phys Oceanogr 23:452–464

Savijärvi HI (1988) Global energy and moisture budgets from rawinsonde data. Mon Weather Rev 116:417–430

Semtner AJ Jr, Chervin RM (1988) A simulation of the global ocean circulation with resolved eddies. J Geophys Res 93:15502–15522

Semtner AJ Jr, Chervin RM (1992) Ocean general circulation from a global eddy-resolving model. J Geophys Res 97:5493–5550

Stephens GL, Campbell CG, Vonder Haar TH (1981) Earth radiation budgets. J Geophys Res 86:9739–9760

Stone PH, Risbey JS (1990) On the limitations of general circulation climate models. Geophys Res Lett 17:2173–2176

Trenberth KE (1979) Mean annual poleward energy transports by the oceans in the Southern Hemisphere. Dyn Atmos Ocean 4:57–64

Trenberth KE (1987) The role of eddies in maintaining the westerlies in the southern hemisphere winter. J Atmos Sci 44:1498–1508

Trenberth KE (1991) Climate diagnostics from global analyses: conservation of mass in ECMWF analyses. J Clim 4:707–722

Trenberth KE (1992) Global analyses from ECMWF and atlas of 1000 to 10 mb circulation statistics. NCAR Tech Note NCAR/TN-373+STR

Trenberth KE, Olson JG (1988) An evaluation and intercomparison of global analyses from NMC and ECMWF. Bull Am Meteorol Soc 69:1047–1057

Trenberth KE, Branstator GW (1992) Issues in establishing causes of the 1988 drought over North America. J Clim 5:159–172

Trenberth KE, Large WG, Olson JG (1990) The mean annual cycle in global ocean wind stress. J Phys Oceanogr 20:1742–1760

Trenberth KE, Berry JC, Buja LE (1993) Vertical interpolation and truncation of model-coordinate data. NCAR Tech Note NCAR/TN-396+STR

Vonder Haar TH, Oort AH (1973) A new estimate of annual poleward energy transport by the oceans. J Phys Oceanogr 3:169–172

Weare BC (1989) Uncertainties in estimates of surface heat fluxes derived from marine reports over the tropical and subtropical oceans. Tellus 41A:357–370

Weare BC, Strub PT (1981) The significance of sampling biases on calculated monthly mean oceanic surface heat fluxes. Tellus 33:211–224

Yanai M, Esbensen S, Chu J-H (1973) Determination of bulk properties of tropical cloud clusters from large-scale heat and moisture budgets. J Atmos Sci 30:611–627

Yanai M, Chu J-H, Stark TE, Nitta T (1976) Response of deep and shallow tropical maritime cumuli to large-scale processes. J Atmos Sci 33:976–991

Yanai M, Li C, Song Z (1992) Seasonal heating of the Tibetan plateau and its effects on the evolution of the Asian summer monsoon. J Meteorol Soc Japan 70:319–351